PFG

Photogrammetrie Fernerkundung Geoinformation

Journal for Photogrammetry, Remote Sensing and Geoinformation Science

Organ der Deutschen Gesellschaft für Photogrammetrie, Fernerkundung und Geoinformation (DGPF) e. V.

Jahrgang 2016, Heft 1

E. Schweizerbart'sche Verlagsbuchhandlung
(Nägele u. Obermiller) Stuttgart 2016

Deutsche Gesellschaft für Photogrammetrie, Fernerkundung
und Geoinformation (DGPF) e.V.
Gegründet 1909

Die *Deutsche Gesellschaft für Photogrammetrie, Fernerkundung und Geoinformation* (DGPF) e.V. unterstützt als Mitglieds- bzw. Trägergesellschaft die folgenden Dachverbände:

International Society
for Photogrammetry
and Remote Sensing

Deutsche Arbeits-
gemeinschaft für
Mustererkennung e.V.

GeoUnion
Alfred-Wegener-Stiftung

Herausgeber:

Präsident: Prof. Dr. Thomas Kolbe, Technische Universität München, Institut für Geodäsie, GIS und Landmanagement, Lehrstuhl für Geoinformatik, Arcisstraße 21, 80333 München, Germany, Tel. +49-89-289-23888
Geschäftsstelle: Tanja Nyc, c/o Technische Universität München, Institut für Geodäsie, GIS und Landmanagement, Lehrstuhl für Geoinformatik, Arcisstraße 21, 80333 München, Germany, Tel.: +49-89-289-22578, e-mail: geschaeftsstelle@dgpf.de

Published by: E. Schweizerbart'sche Verlagsbuchhandlung (Nägele u. Obermiller), Johannesstraße 3A, 70176 Stuttgart, Germany, Tel.: +49-711 351456-0, Fax: +49-711 351456-99, e-mail: mail@schweizerbart.de
Internet: http://www.schweizerbart.de

♾ Gedruckt auf alterungsbeständigem Papier nach ISO 9706-1994

ISSN 1432-8364 / e-ISSN 2363-7145

Science Citation Index Expanded (also known as SciSearch®) Journal Citation Reports/Science Edition

Erscheinungsweise: 6 Hefte pro Jahrgang.
Bezugspreis im Abonnement: € 262,– pro Jahrgang. Mitglieder der DGPF erhalten die Zeitschrift kostenlos. Der Online-Zugang ist im regulären Subskriptionspreis enthalten.
Anzeigenverwaltung: E. Schweizerbart'sche Verlagsbuchhandlung (Nägele u. Obermiller), Johannesstraße 3A, 70176 Stuttgart, Germany, Tel.: +49-711 351456-0; Fax: +49-711 351456-99.
e-mail: mail@schweizerbart.de, Internet: http://www.schweizerbart.de
Bernhard Harzer Verlag GmbH, Westmarkstraße 59/59a, 76227 Karlsruhe, Germany, Tel.: +49-721 944020, Fax: +49-721 9440230, e-mail: Info@harzer.de, Internet: www.harzer.de
Printed in Germany by Tutte Druckerei & Verlagsservice GmbH, 94121 Salzweg, Germany.

PFG – Jahrgang 2016, Heft 1
Inhaltsverzeichnis

Originalbeitrag

Beiträge aus Wissenschaft und Praxis

Mitteilungen

Zusammenfassungen der „Originalbeiträge“ und der „Beiträge aus Wissenschaft und Praxis“ (deutsch und englisch) sind auch verfügbar unter www.dgpf.de/neu/pfg/ausgaben.htm

PFG 2016 / 1, 005–015
Stuttgart, February 2016

Article

Automatic Generation of Orthorectified High Resolution Satellite Imagery – a Case Study for Saudi Arabia

Muhamad Alrajhi, Riyadh, Saudi Arabia & Christian Heipke, Hannover

Keywords: Orthophotos, satellite imagery, high resolution, image matching

Summary: The Ministry of Municipal and Rural Affairs (MOMRA) is responsible for the production, maintenance and delivery of accurate geospatial data for all urban and rural settlements in the Kingdom of Saudi Arabia. The fast urbanization requires up-to-date information, which is a major challenge. High resolution satellite imagery presents a novel and promising data resource for geospatial data update. It is well-known that a satellite image, if georeferenced using the vendor-provided rational polynomial coefficients (RPC), often displays X- and Y-coordinate biases of several pixels. Ground control points (GCP) are typically required to achieve an accuracy at pixel level. The collection of the 3D coordinates of GCP and their corresponding image coordinates is a time consuming and cost intensive manual process.

The primary objective of this research is to use image matching between existing orthophotos and the satellite images, georeferenced with RPC instead of GCP, in order to automate and speed up the orthorectification process. Based on a series of practical experiments using imagery from GeoEye and IKONOS, the potential of automated matching between aerial and satellite images using the well known Speeded-Up Robust Features (SURF) algorithm for the described task is investigated. The matched points serve as a basis for transforming the satellite orthophoto to the aerial orthophoto using a 2D affine transformation.

This research has led to the development of a simple and efficient tool for satellite imagery with a ground sampling distance of 50 cm to 1 m to be used for updating geospatial information that meets MOMRA accuracy standards for 1:10,000 scale mapping. The process completely eliminates the need for GCP. About 12 to 15 satellite images are routinely being processed on a workstation in a single day. The implementation of this tool at MOMRA greatly enhances its ability to quickly respond to urgent needs for updated geospatial data.

Zusammenfassung: *Automatische Erzeugung orthorektifizierter hoch aufgelöster Satellitenbilder – Pilotprojekt für Saudi Arabien*. Das Ministry of Municipal and Rural Affairs (MOMRA) ist für die Erstellung, Laufendhaltung und Bereitstellung von genauen Geoinformationen für alle städtischen und ländlichen Siedlungen des Königreichs Saudi Arabien verantwortlich. Die schnelle Urbanisierung erfordert aktuelle Informationen, was eine große Herausforderung darstellt. Hoch aufgelöste Satellitenbilder stellen eine neue, viel versprechende Datenquelle für die Aktualisierung räumlicher Daten dar. Bekanntlich zeigen Satellitenbilder, die mit Hilfe der von den Satellitenbetreibern bereitgestellten Rationalen Polynomkoeffizienten (RPC) georeferenziert wurden, oft Systematiken in den X- und Y-Koordinaten im Bereich mehrerer Pixel. Typischerweise werden Passpunkte benötigt, um eine Genauigkeit im Bereich eines Pixels zu erzielen. Die Bestimmung der Passpunktkoordinaten im Bild- und Objektraum ist ein zeitaufwändiger und kostspieliger manueller Prozess.

Das wesentliche Ziel der hier vorgestellten Arbeiten ist die Nutzung von Bildzuordnungsverfahren zwischen existierenden Orthophotos und den mit RPC georeferenzierten Satellitenbildern anstelle der Passpunkte, um die Orthoprojektion zu automatisieren und zu beschleunigen. Auf der Grundlage einer Reihe praktischer Experimente mit Daten der Satelliten GeoEye und IKONOS wird das Potenzial des bekannten Speeded-Up Robust Features (SURF) Algorithmus für die gestellte Aufgabe untersucht. Die zugeordneten Verknüpfungspunkte dienen als Eingangswerte für eine 2D Affintransformation zur Verbesserung der Position des Satellitenbildes.

Die Forschungen haben zur Entwicklung einer einfachen und effizienten Software für die Orthoprojektion von Satellitenbildern mit einer Bodenauflösung im Meterbereich geführt. Die Software wird für die Aktualisierung räumlicher Daten genutzt, die die Anforderungen von MOMRA an Kartierungen im Maßstab 1:10,000 erfüllt. Der

www.schweizerbart.de
DOI: 10.1127/pfg/2016/0285
1432-8364/16/0285 $ 2.75

Prozess benötigt keinerlei Passpunkte. 12 bis 15 Satellitenbilder können pro Tag routinemäßig auf einem Arbeitsplatz prozessiert werden. Die Implementierung in MOMRA verbessert die Möglichkeit, schnell auf dringende Bedürfnisse im Hinblick auf aktuelle räumliche Daten reagieren zu können, erheblich.

1 Introduction

Up-to-date geospatial data play a key role in decision making, planning and sustainable development of any geographic region. A most essential need is to provide timely supplements to existing data. Rapid development of infrastructure, high rate of growth and fast changes in urban and rural areas are the major challenges to maintaining currency in a national geospatial database. These developments call for alternative procedures for economic, accurate and rapid geospatial database updating. As a case study Saudi Arabia presents an example which can provide sufficient material to analyse and develop general updating procedures, which can be used globally.

If the existing topographic maps are not very old and only about 10% to 15% of the features have changed, it is uneconomical to map the entire area through a new aerial survey. In such a case, an alternate methodology that allows the incorporation of only the changes into the existing database is faster and, consequently, more economic. Hence, satellite image based mapping can be considered as an alternative to ground and aerial survey.

The objective of this research is to devise, implement and test a methodology for rapid mapping from recent high resolution satellite imagery (HRSI) which eliminates manual work. The first step consists in georeferencing the images based on vendor-provided rational polynomial coefficients (RPC) and height information. In this article, *georeferencing* only refers to a transformation of satellite images using vendor-provided RPC and a DTM. *Orthorectification* denotes the more precise process including either ground control points or the described matching procedure. Since RPC are typically not accurate enough, control is needed to refine the results. This control is established by image matching between the georeferenced satellite images and existing aerial orthophotos.

The remainder of the paper is organised as follows: section 2 discusses prior work; section 3 contains a detailed description of the devised methodology. In section 4 we present the test data used in our study and report the experimental results. Section 5 concludes the paper.

2 Related Work

2.1 *Georeferencing and Orthorectifying High Resolution Satellite Images*

A review of the literature can be summarized as follows:

- The feasibility of topographic mapping using currently available HRSI has been clearly demonstrated (Gianinetto 2008, Li & Batchvarowa 2008, Holland et al. 2006).
- The basic challenge of sensor orientation of HRSI has largely been solved in previous research (Di et al. 2003, Tao & Hu 2002).
- It has been shown (Fraser & Yamakawa 2004, Grodecki & Dial 2003) that GCP are needed to supplement the vendor-provided RPC to achieve sub-metre positional accuracy required for mapping at large scales from HRSI. Some isolated studies (e.g. Fraser et al. 2002) attempt to establish some correlation between the number of GCP and the resulting map accuracy.
- It is widely recognized that the collection of 3D coordinates for the GCP and their identification in the imagery are the most arduous and time consuming steps in the whole process. Consequently, efforts have been undertaken to automate image orientation using database information. For aer-

ial images, only the contribution by Läbe (1999) using the system AMOR (Automatic Model-based Orientation) reported success. Others (e.g. Karjalainen & Kuittinen 1999, Jedryczka 1999, Pedersen 1999) describe semi-automated interactive solutions, which had less success in operational environments.

More recently, aerial images have been oriented using positioning and attitude information from systems like GPS and inertial measurement units (Blázquez & Colomina 2012). There is, however, a need for seeking alternative methods for the automatic orthoprojection of HRSI.

2.2 *Image Matching of Aerial and Satellite Images*

Image matching has been widely investigated over the last decades and is currently an operational tool for image orientation and the derivation of digital terrain and surface models in photogrammetry and remote sensing (Heipke 1997). In the context of this paper image matching can be employed to substitute the needed GCP by matching the satellite image to an aerial orthophoto.

For image orientation, procedures based on distinctive invariant features, have been reported to be considerably successful in recent

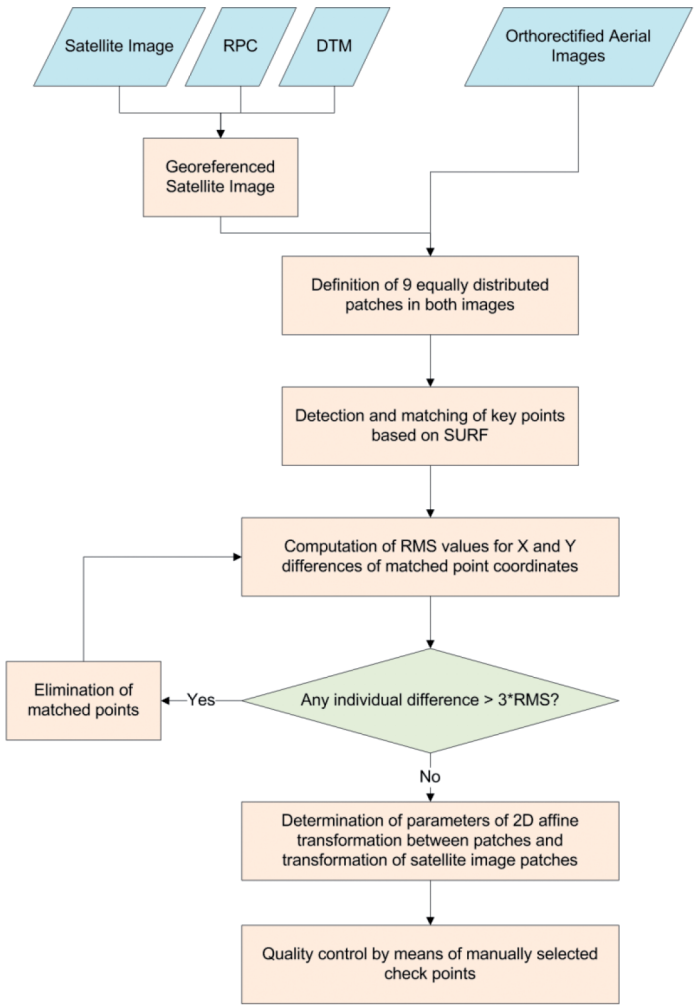

Fig. 1: Workflow diagram.

years. These features need to be invariant to image scale and rotation, limited changes in 3D viewpoint, noise, and changes in illumination. Examples for such routines include the Scale Invariant Feature Transform (SIFT – Lowe 2004) and the Speeded-Up Robust Features (SURF – Bay et al. 2008). Both detectors consist of three steps: feature detection, feature description, and feature matching. As shown in many investigations (e.g. Juan & Gwun 2009), SIFT and SURF are equally robust, but SURF is computationally much faster. Consequently, SURF has been selected for this research.

3 Methodology

As mentioned it is highly desirable that the need for establishing ground control points for mapping from satellite imagery should be entirely eliminated. To serve this purpose, the most useful data in Saudi Arabia are existing digital orthophotos with 50 cm ground sampling distance (GSD) derived from 1:45,000 scale aerial imagery (Alrajhi 2013). The orthophotos have a geometric accuracy in the range of the GSD. Although this is less than desired, it can still be expected that the orthophotos provide effective control to refine the RPC orientation of the HRSI, if enough matched points are available.

For matching of the GeoEye and IKONOS imagery with the orthophotos, we face the combined challenge of multi-sensor and multi-scale image matching. The images were typically also acquired at different times, and thus in principle multi-seasonal effects come to play. However, our test sites only varied slightly within the year which eliminated the need to cope with such seasonal alterations.

First, the HRSI are georeferenced based on the vendor-provided RPC and a digital terrain model (DTM). In order to refine this approximate result, SURF is used to locate and match key points on these satellite and overlapping aerial orthophotos. As the coverage of an IKONOS scene is 11 × 11 km^2 and that of GeoEye imagery is 10 × 10 km^2, it is rather resource consuming to determine key points in the whole satellite scene and the overlapping orthophoto, respectively. To speed up the process, we only use nine equally distributed subwindows of 800 × 800 pixels extracted from the corresponding pairs of satellite and aerial images. In each sub-window, the number of key points is restricted to a maximum of 200. Then, the matching procedure is applied in the neighbourhood of some 10 × 10 pixels for each key point extracted in the aerial orthophoto. The coordinates of the matched point pairs are subsequently compared to eliminate gross matching errors: The RMS values for the X-coordinate and the Y-coordinate differences are calculated and pairs showing a difference larger than 3 times the RMS value are rejected.

Next, the satellite image is precisely transformed to the geometry of the orthophoto. Even though the differences in the two coordinate datasets are likely to be dominated by X- and Y-coordinate shifts (Fraser & Yamakawa 2004, Dowman et al. 2012), a 2D affine transformation with six parameters is used in this step. The large number of matched key points, if well distributed over the image, results in a strong least squares based adjustment solution. In addition, the adjustment residuals provide further information regarding the image matching success. A final check based on manually selected check points ensures a high quality of the final product. The described procedure is shown in Fig. 1.

4 Experimental Results

4.1 *Test Sites*

The proposed automated orthoprojection process was tested over the different landscapes of Saudi Arabia visible in the IKONOS and GeoEye satellite images. Three separate sites were selected for this purpose. Test area 1 contains a densely urbanized part of southwestern Riyadh as well as the adjoining suburban area which is undergoing rapid new development. Test area 2, Al Muzahimiyah, is located about 25 km to the south-west of Riyadh along an escarpment. It includes several cultivated farm parcels and shows a significant variation in topography in a rural landscape. Test area 3, Huraymila, is a small city located about 90 km from Riyadh, surrounded with old style farms

with a lot of palm trees. The landscape in the test site ranges from acacia covered wadis to pronounced escarpments and wide plains. The HRSI available for the test are described in Tab. 1. In all cases pan-sharpened images were used.

4.2 *Results*

Tests were conducted for all three test sites and for all images listed in Tab. 1. To illustrate the results, we present details of the test site Riyadh for the GeoEye and IKONOS images of 2010 (see Figs. 2 to 5); the other results look rather similar.

Riyadh, GeoEye 2010 imagery: Fig. 2 depicts a thumbnail view of the GeoEye image. The nine equally distributed 800 × 800 pixel image patches are highlighted in yellow colour. Fig. 3 contains the distribution of the automatically selected points for three selected patches of Fig. 2 (left patch of upper row, centre patch of middle row, centre patch of lower row). It has to be noted that radiometric differences are taken into account within SURF. It can be seen that in all cases a large number of well distributed points was found. The second

Tab. 1: GeoEye (left) and IKONOS (right) images used in the study.

Area	Date of Imaging
Riyadh	20 Nov 2009
Riyadh	01 May 2010
Al Muzahimiyah	26 Nov 2009
Al Muzahimiyah	09 Jan 2010

Area	Date of Imaging
Riyadh	09 Aug 2008
Riyadh	01 May 2010
Al Muzahimiyah	25 Nov 2008
Huraymila	28 Dec 2009

Tab. 2: Number and distribution of matched points, GeoEye 2010 image.

Image patch	Area type	No. of matched points
Upper left	Open	77
Upper centre	Open	38
Upper right	Open	33
Middle left	Agriculture	125
Middle centre	Built-up	184
Middle right	Built-up	174
Lower left	Built-up	140
Lower centre	Built-up	182
Lower right	Agriculture	147
SUM		**1100**

Fig. 2: Riyadh, GeoEye image 2010; location of nine image patches.

Tab. 3: RMS values for check points, GeoEye 2010 image.

Area type	No. of check points	RMS_X (m)	RMS_Y (m)
Total satellite image	20	0.61	0.75
Open area	7	0.48	0.57
Built-up area	8	0.75	0.76
Agriculture area	5	0.57	0.89

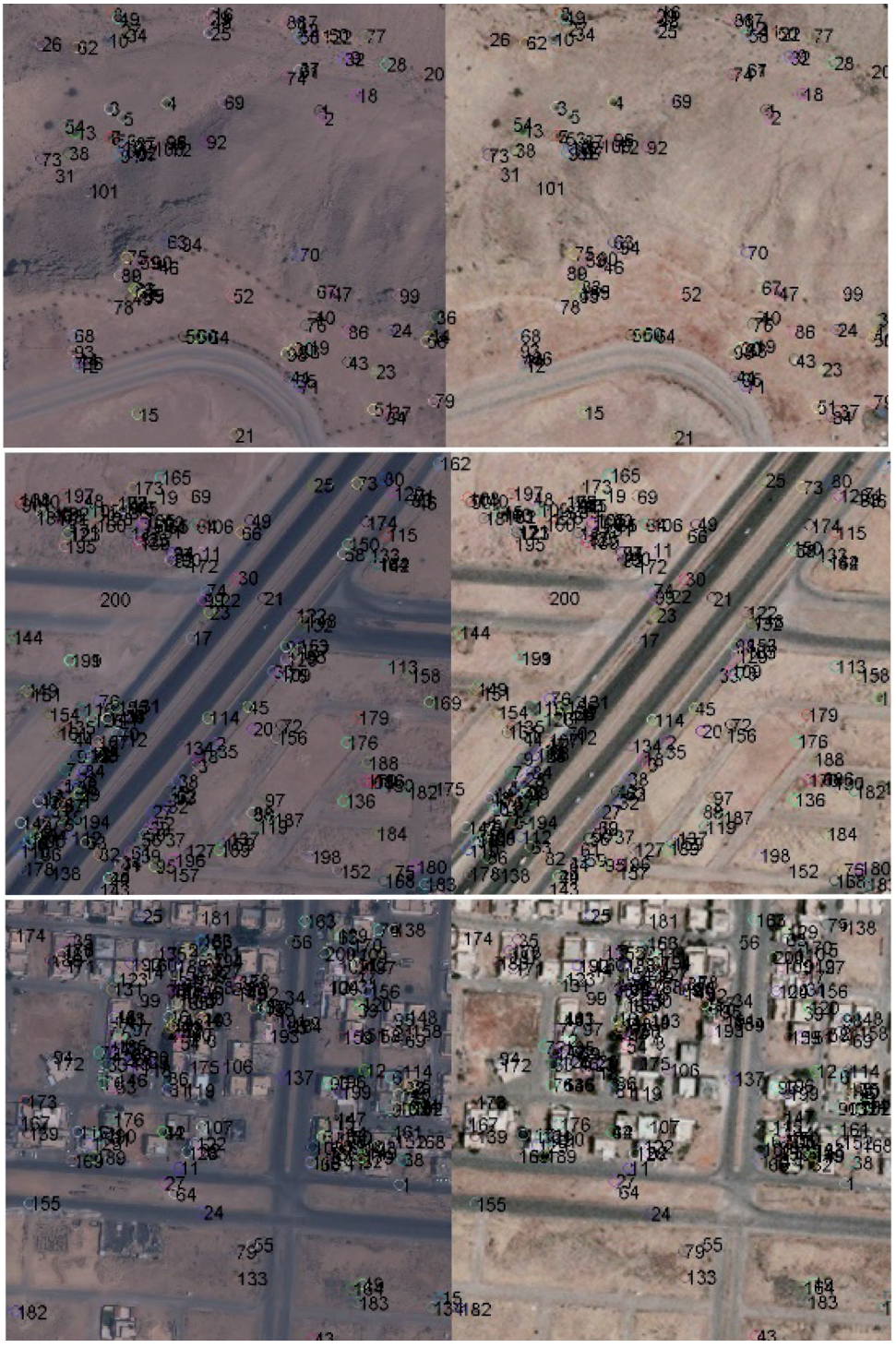

Fig. 3: Distribution of matched points for three selected image patches (left GeoEye image, right orthophoto) shown in Fig. 2: left patch of upper row (open), centre patch of middle row (built-up), centre patch of lower row (built-up).

and the third patch, which depict urban areas with comparatively high texture, show more points, which is not surprising.

Numerical results are presented in Tabs. 2 and 3. Tab. 2 characterises each patch and lists the number of matched points. For all terrain types, numerous points are found. In total, 1,100 matching points were available, which is of course more than enough for the 2D subsequent affine transformation. Tab. 3 contains the RMS values at independent check points for different area types and shows that an accuracy in the range of about 1.2 pixels was reached, which is reasonable, since the image coordinates of the check points were digitised in the 50 cm orthophotos. The mean differences vanish for both the X- and the Y-axis, indicating a fit between satellite and aerial orthophoto without any systematic errors.

Riyadh, IKONOS 2010 imagery: Results are displayed for the IKONOS 2010 image of test site Riyadh which has a GSD of 1 m. Fig. 4 contains a thumbnail of the image with the location of the nine patches used for matching. For two examples Fig. 5 shows the detailed distribution of the matched points, again it can be seen that a large number of well distributed points was found. Numerical results are contained in the following tables. Tab. 4 characterises each patch and lists the number of matched points; in total more than 1,200 points were used, which is nearly 10% more than for the GeoEye image. The reason is probably the larger proportion of built-up area in the image patches, exhibiting stronger image texture. Tab. 5 contains the RMS values at the check points and in general confirms the findings for the GeoEye image. Again an accuracy of about 1.2 pixels was reached in most cases, although the differences in Y are a little higher for open and agricultural area, probably due to poor texture. The mean differences again vanish, which means that the observations do not contain any systematic errors.

Tab. 6 contains the RMS values derived at check points, differentiated according to the

Tab. 4: Number of matched points, IKONOS image.

Image patch	Area type	No. of matched points
Upper left	Built-up	108
Upper centre	Built-up / agricult.	116
Upper right	Built-up/ open	187
Middle left	Built-up / agricult.	30
Middle centre	Built-up	162
Middle right	Built-up / agricult.	134
Lower left	Open	101
Lower centre	Open	168
Lower right	Open	196
SUM	-	**1202**

Fig. 4: Riyadh, IKONOS image 2010; location of image patches.

Tab. 5: RMS values for check points, IKONOS image.

Area	No. of check points	RMS_X (m)	RMS_Y (m)
Total satellite image	20	1.17	1.61
Open area	6	1.20	1.85
Built-up area	9	1.15	1.32
Agriculture area	5	1.17	1.64

area types built-up, agricultural and open for all eight images listed in Tab. 1. All values range from 1 to 1.5 GSD which again confirms the findings already discussed. In units of the GSD the values for the IKONOS images were smaller than those for the GeoEye images; this points to the fact that, as expected, the matching procedure delivers sub-pixel accuracy. The lower accuracies for GeoEye images reported in Tab. 6 (GSD) is mainly a result of the manual digitisation of the check points in the aerial orthophotos which negatively influenced geometric accuracy. Again, the mean differences all vanish.

The test results have convincingly demonstrated that SURF provides a very effective image matching approach for multi-scale and multi-sensor image matching. As pointed out

Fig. 5: Distribution of matched points for left (built-up) and right (built-up/open) image patch of the upper row shown in Fig. 4 (left IKONOS image, right: orthophoto).

Tab. 6: RMS values for check points, all test images.

Satellite Image	Built-up		Agricultural		Open	
	RMS_X (m)	RMS_Y (m)	RMS_X (m)	RMS_Y (m)	RMS_X (m)	RMS_Y (m)
GeoEye, Riyadh 2009	0.71	0.81	0.61	0.85	0.56	0.68
GeoEye, Riyadh 2010	0.75	0.79	0.58	0.91	0.46	0.58
GeoEye, Al Muzahimiyah 2009	0.68	0.75	0.54	0.83	0.52	0.65
GeoEye, Al Muzahimiyah 2009	0.73	0.85	0.63	0.87	0.59	0.63
IKONOS, Riyadh 2008	0.94	1.22	0.98	1.29	1.09	1.38
IKONOS, Riyadh 2010	1.05	1.27	1.15	1.57	1.14	1.42
IKONOS, Al Muzahimiyah 2008	1.25	1.31	1.18	1.34	1.17	1.46
IKONOS, Huraymila 2009	1.32	1.29	1.07	1.24	1.21	1.34

earlier, the use of the vendor-provided RPC data often results in systematic georeferencing errors. These are effectively corrected by the two shift parameters of the affine transformation that have the dominating influence on the transformation. In fact, it may often be sufficient to simply apply these two shift parameters. The 2D affine transformation also presents another opportunity to filter out poorly matched key points. A threshold of 3 times the RMS_X and RMS_Y values, respectively, was used for rejecting poorly matched points in this study, which due to the large number of matched points provided sufficiently accurate and reliable results.

5 Conclusions

Maintenance and delivery of geospatial information by MOMRA serves the needs of a large number of national and regional government agencies in Saudi Arabia. Line maps and orthophoto maps produced at scale 1:10,000 are most commonly used for regional planning, they must meet accuracy standards of 1.25 m in both planimetric coordinates at the 1-σ level. Accordingly, any conclusions about the impact of this research study on the enhanced capability of MOMRA for rapidly updating with the use of recently acquired high resolution satellite imagery should be drawn in the light of the information needs mentioned.

Based on the analysis of the results obtained with the experiments reported in this paper, the following conclusions can be drawn:

- The existing aerial 50 cm resolution orthophoto database can effectively be used as control for the orthorectification of satellite imagery of 50 cm to 1 m GSD in order to generate updated 1:10,000 scale line maps and orthoprojected 50 cm and 1 m resolution images that meet MOMRA map accuracy standards.
- In order to generate these products, coordinates for 15 or more control points that are well distributed across the image, may be obtained through manual measurements on the existing orthophotos and the new satellite images and combined with the RPC and DTM data for the orthoprojection of the satellite image. About 4 to 5 hours of a trained operator time is required to complete this process.
- A more efficient alternative for orthorectifying of the new satellite images is based only on the vendor-supplied RPC and DTM data, a process which can usually be completed within one hour. The resulting georeferenced satellite image is then matched with the corresponding existing aerial orthophoto using the proposed SURF-based matching that generates a large number of matched points. These points are subsequently used to transform the satellite image to the orthophoto geometry via a 2D affine transformation. SURF matching and

coordinate transformation only takes a few minutes and results in an orthorectified satellite image that meets MOMRA map accuracy standards for 1:10,000 scale mapping.

- The orthoprojection of a new satellite image can be carried out at a production rate of 12 to 15 satellite images per day without the need for neither field control nor measurement of image coordinates by a skilled human operator. Hence, a viable solution for orthophoto generation in MOMRA's map production environment is now available, in complete fulfilment of the primary objective for this research.
- Based on the currently available 50 cm resolution orthophotos the proposed procedure can be used for generating orthophotos that meet the MOMRA accuracy standard for 1:10,000 map scale. However, if aerial orthophotos of higher positional accuracy become available for control, the proposed procedure will be applicable for generating up-to-date satellite orthophotos of correspondingly higher accuracy.

There are several uses of geospatial information where the completeness and the validity of the map data is of primary interest while the geometric accuracy is of secondary importance. For example, due to the rapid pace of urbanization in Saudi Arabia, the planning for continued urban development requires frequent updating of the land use map that is most commonly compiled from the 1:2,500 scale map database of MOMRA. Such land use planning can be greatly facilitated if MOMRA can rapidly deliver geospatial information that has been updated using recently acquired satellite imagery. Hence and despite not meeting MOMRA's geometric map accuracy standards for land use mapping at the 1:2,500 scale, the up-to-date satellite images can be of paramount importance for spatial planning in Saudi Arabia, as they represent topologically correct current information.

References

Alrajhi, M., 2013: A Semi-Automated Procedure for Orthophoto Generation from High Resolution Satellite Imagery. – Wissenschaftliche Arbeiten der Fachrichtung Geodäsie und Geoinformatik der Leibniz Universität Hannover Nr. 307.

Bay, H., Ess, A., Tuytelaars, T. & van Gool, L., 2008: SURF: Speeded-Up Robust Features. – Computer Vision and Image Understanding **110** (3): 346–359.

Blázquez, M. & Colomina, I., 2012: Relative INS/GNSS aerial control in integrated sensor orientation: models and performance. – ISPRS Journal of Photogrammetry and Remote Sensing **67:** 120–133.

Di, K., Ma, R. & Li, R., 2003: Rational functions and potential for rigorous sensor model recovery. – Photogrammetric Engineering and Remote Sensing **69** (1): 33–41.

Dowman, I., Jacobsen, K., Konecny, G. & Sandau, R., 2012: High Resolution Optical Satellite Imagery. – Whittles Publishing, Caithness, UK.

Fraser, C., Hanley, H.B. & Yamakawa, T., 2002: Three-dimensional geopositioning accuracy of IKONOS imagery. – Photogrammetric Record **17** (99): 465–479.

Fraser, C. & Yamakawa, T., 2004: Insights into the affine model for high-resolution satellite sensor orientation. – ISPRS Journal of Photogrammetry and Remote Sensing **58:** 275–288.

Gianinetto, M., 2008: Updating Large Scale Topographic Databases in Italian Urban Areas with Submeter QuickBird Images. – International Journal of Navigation and Observation: 116–124.

Grodecki, J. & Dial, G., 2003: Block adjustment of high-resolution satellite images described by rational polynomials. – Photogrammetric Engineering and Remote Sensing **69** (1): 59–70.

Heipke, C., 1997: Automation of interior, relative and absolute orientation. – ISPRS Journal of Photogrammetry and Remote Sensing **52** (1): 1–19.

Holland, D., Boyd, D. & Marshall, P., 2006: Updating topographic mapping in Great Britain using imagery from high-resolution satellite sensors. – ISPRS Journal of Photogrammetry and Remote Sensing **60:** 212–223.

Jedryczka, R., 1999: Contribution to OEEPE-test on automatic orientation of aerial images. – Task A-Semi-Automatic Exterior Orientation Using Existing Vector Map Data, OEEPE **36:** 133–137.

Juan, L. & Gwun, O., 2009: A comparison of SIFT, PCA-SIFT and SURF. – International Journal of Image Processing **3** (4):143–152.

Karjalainen, M. & Kuittinen, R., 1999: Contribution to OEEPE-test on automatic orientation of aerial images. – Task A-interactive Exterior Orientation Using Linear Features from Vector Maps, OEEPE **36:** 127–131.

Läbe, T., 1999: Contribution to OEEPE-test on automatic orientation of aerial images. – Task A-Experiences with AMOR, OEEPE **36:** 119–126.

Li, A. & Batchvarova, T., 2008: Topographic mapping and terrain modeling from multi-sensor satellite imagery. – International Archives of Photogrammetry, Remote Sensing and the Spatial Information Sciences **XXXVI**, Part 1: 809–814.

Lowe, D., 2004: Distinctive image features from scale-invariant keypoints. – International Journal of Computer Vision **60** (2): 91–110.

Pedersen, B., 1999: Contribution to OEEPE-test on automatic orientation of aerial images. – Task A-Solution from Alborg, OEEPE **36:** 139–144.

Tao, V. & Hu, Y., 2002: 3D reconstruction methods based on the rational function model. – Photogrammetric Engineering and Remote Sensing **68** (7): 705–714.

Addresses of the Authors:

Prof. Dr.-Ing. Muhamad Alrajhi, Ministry of Municipal and Rural Affairs (MOMRA), Deputy Minister for Land & Surveying, P.O.Box 89936, 11692 Riyadh, Saudi Arabia.

Prof. Dr.-Ing. habil. Christian Heipke, Leibniz Universität Hannover, Institut für Photogrammetrie und GeoInformation, Nienburger Str. 1, 30167 Hannover, Germany, e-mail: heipke@ipi.uni-hannover.de

Manuskript eingereicht: Juni 2015
Angenommen: Dezember 2015

PFG 2016 / 1, 017–030
Stuttgart, February 2016

Article

Accuracy Analysis of Photogrammetric UAV Image Blocks: Influence of Onboard RTK-GNSS and Cross Flight Patterns

Markus Gerke, Enschede, The Netherlands & Heinz-Jürgen Przybilla, Bochum

Keywords: self-calibration, (in)direct sensor orientation, block deformation, UAV-based RTK, cross flight pattern, sensor synchronisation

Summary: Unmanned aerial vehicles (UAV) are increasingly used for topographic mapping. Despite the flexibility gained when using those devices, one has to invest more effort for ground control measurements compared to conventional photogrammetric airborne data acquisition, because positioning devices on UAVs are generally less accurate. Additionally, the limited quality of employed end-user cameras asks for self-calibration, which might cause some problems as well. A good distribution of ground control points (GCPs) is not only needed to solve for the absolute orientation of the image block in the desired coordinate frame, but also to mitigate block deformation effects which are resulting mainly from remaining systematic errors in the camera calibration. In this paper recent developments in the UAV-hardware market are picked up: some providers equip fixed-wing UAVs with RTK-GNSS-enabled 2-frequency receivers and set up a processing pipeline which allows them to promise an absolute block orientation in a similar accuracy range as through traditional indirect sensor orientation. Besides the analysis of the actually obtainable accuracy, when one of those systems is used, we examine the effect different flight directions and altitudes (cross flight) have onto the bundle adjustment. For this purpose two test areas have been prepared and flown with a fixed-wing UAV. Results are promising: not only the absolute image orientation gets significantly enhanced when the RTK-option is used, also block deformation is reduced. However, remaining offsets originating from time synchronization or camera event triggering should be considered during flight planning. In flat terrains a cross flight pattern helps to enhance results because of better and more reliable self-calibration.

Zusammenfassung: *Genauigkeitsuntersuchung von photogrammetrischen UAV-Bildverbänden: Einfluss von onboard RTK-GNSS und Kreuzflugmustern.* Flugroboter (unmanned aerial vehicles, UAV) werden zunehmend zur topographische Kartierung eingesetzt. Die Systeme weisen eine hohe Flexibilität auf, jedoch muss im Gegensatz zu konventionellen Befliegungen mehr Aufwand in die Erfassung von Kontrollpunkten am Boden investiert werden. Der Grund dafür liegt in der schlechteren Qualität der Positionierungslösungen auf dem Flugroboter. Hinzu kommt, dass die verwendeten Kameras eine unbekannte geometrische Stabilität haben, und die Parameter der Inneren Orientierung normalerweise nicht hinreichend genau fixiert sind. Die Folge ist, dass eine Selbstkalbrierung im Rahmen der Bündelausgleichung durchgeführt werden muss. Diese Selbstkalibrierung ist nicht in jedem Anwendungsfall zuverlässig. Eine gute Verteilung von Kontrollpunkten ist nicht nur für die Bestimmung der Lagerung des Bildverbandes notwendig sondern auch um Blockdeformationen zu verringern. Diese entstehen größtenteils durch bei der Kamerakalibrierung verbliebene systematische Fehler. In diesem Beitrag greifen wir aktuelle Entwicklungen im UAV-Markt auf: einige Hersteller rüsten ihre Geräte mit einem RTK-fähigen 2-Frequenz-GNSS-Empfänger aus und bieten einen entsprechenden Prozessierungsablauf an. Sie versprechen dadurch Genauigkeiten in einem Bereich ähnlich der traditionellen indirekten Sensorpositionierung zu erhalten. Neben der Analyse der tatsächlich erreichbaren Genauigkeit eines dieser Systeme untersuchen wir den Effekt, den verschiedene Flugrichtungen und -höhen auf die Blockausgleichung haben (Kreuzbefliegung). Zu diesem Zweck wurden zwei Testareale vorbereitet und mit einem unbemannten Flächenflugzeug beflogen. Die Ergebnisse sind vielversprechend: durch die Nutzung der RTK-Option wird nicht nur die absolute Blockorientierung signifikant verbessert, auch werden

www.schweizerbart.de
DOI: 10.1127/pfg/2016/0284
1432-8364/16/0284 $ 3.50

die Blockdeformationen reduziert. Es sollten jedoch verbleibende Fehler, die durch ungenaue Synchronisation der Sensorbeobachtungen oder Kameraauslösung entstehen, bei der Flugplanung berücksichtigt werden. In flachen Gebieten hilft die Kreuzbefliegung die Ergebnisse zu verbessern, da eine bessere und zuverlässigere Selbstkalibrierung durchgeführt werden kann.

1 Introduction

The derivation of topographic information from unmanned aerial vehicles (UAV) is becoming increasingly interesting for routine tasks in the geomatics domain. Digital surface models (DSM) or ortho images are standard products. Especially for the acquisition of relatively large image blocks (some 100+ hectares) small fixed-wing UAVs are used (Colomina & Molina 2014). In this paper we use the term UAV, but in literature we find also terms like UAS (unmanned aerial system) or RPAS (remotely piloted aerial system). In the scope of this article all those abbreviations are treated as synonyms. More specifically we refer to small UAV which are devices with an overall weight of up to 25 kg (Nex & Remondino 2014, Watts et al. 2012). Small UAVs being easily deployed require only small training efforts and in many countries regulations are in place which allow for a convenient permission issuance.

The main advantages of small UAVs over traditional (manned) airborne-based mapping are: i) flexibility – individual flight patterns can be realized; ii) unrivalled image resolution – a ground pixel size of 5 cm, mostly smaller, can easily be achieved; iii) ease of use – with a small training effort, state-of-the-art devices can be operated even by laymen. However, compared to established workflows based on manned airborne photography, some issues need to be considered. Because of weight and cost restrictions, sensor devices used in UAVs (positioning, camera) are normally of much lower quality compared to professional sensors employed in manned airborne systems. This has as the consequence that in order to achieve the best accuracy for the final mapping product, a significant amount of work concerning signalization and measurement of ground control points (GCPs) is needed. In this context some recent developments concerning GNSS localization are interesting: there is the tendency towards RTK (Real Time Kinematic) devices being integrated onboard commercially available UAV. This means that in fact, survey-grade direct sensor positioning of UAV images is available for the mass market. Opposed to DGPS, which only considers code-based observations in addition to differential corrections, the RTK approach incorporates phase measurements which promise an absolute accuracy in the sub-cm range.

Another issue to be addressed when capturing UAV-based image blocks is the necessity to estimate intrinsic camera parameters during bundle adjustment (self-calibration). This process adds another source of uncertainty, because the physical stability of the camera as such is unknown. Moreover, if the area of interest is largely flat, the estimate of the principal distance might be very inaccurate due to the high correlation of the Z-component and focal length in nadir viewing geometry. From literature we know that so-called cross flight patterns and different flying heights might render the self-calibration process more reliably (Cramer 2001).

In this paper we present results from experiments which were conducted in several setups in order to address the practically relevant questions concerning a) the influence of cross flight patterns on the overall bundle block adjustment quality and b) the role of GCP distribution on the ground, especially in conjunction with using a RTK-GNSS-enabled commercial fixed-wing UAV. In addition, we analyse the impact those different configurations have on the camera self-calibration.

In an earlier work by Przybilla et al. (2015) already some of the points were addressed. In the paper at hand the experiments are explained in more detail and extended towards a more quantitative evaluation of the RTK-based localization solution and different flight configurations. To this end, several test scenarios, applied in different terrain, are defined and analysed.

In the next section some related research on UAV image block orientation, both using indirect methods, but also referring to onboard positioning solutions, is described. Section 3 elaborates on the data processing workflow as implemented by the system used in our experiments. The subsequent section describes the datasets used, while section 5 focusses on the results. The last section provides some discussion and conclusions.

2 Related Work

In many related papers the usage of GCPs to support indirect sensor orientation of UAV-based image blocks is analysed. One consideration refers to the positional accuracy which is needed at GCPs.

If pixel-level absolute accuracy is aimed for in image orientation, it implies a need for appropriate reference information. Nowadays, a GSD of 2 cm – 3 cm is easily achievable in UAV projects, meaning that 3D points on the ground need to be measured with at least state-of-the-art GNSS-RTK technology or engineering surveying methods based on total stations. In addition there is a need to differentiate between approaches which only apply a 3D-similarity transform to the entire UAV-image block and those which employ control information within the bundle block adjustment, e.g. as soft constraints. The former one is in principle easier to realize but keeps the risk that block deformations within the initial UAV-solution do not get adjusted (Nex & Remondino 2014). In other papers, large errors are reported especially in the Z-component when only a 3D-similary transform is performed (Nocerino et al. 2013, Rumpler et al. 2014). When GCPs were introduced into the bundle adjustment the errors were reduced by a factor of 3, and they became even smaller when oblique images were used. Those oblique images provide an image block geometry which also supports self-calibration (Nocerino et al. 2013).

However, to reduce the workload when dealing with UAV campaigns the desire to obtain reliable results, but without large effort on ground control measurements, is obvious. In literature we find many different approaches to obtain reliable and accurate image orientation parameters within the given mapping frame, but without the use of GCPs and advanced onboard positioning hardware. Förstner & Steffen (2007) used an existing DSM to fine-register an UAV-block based on the UAV-derived DSM. Although they achieved overall good quality in their experiment, the block deformation issue remains unsolved and the requirements on the terrain as such are quite demanding, because the terrain structure should show height gradients in different directions and of different strength to allow for an unambiguous and adequate co-registration. More recently, Yang & Chen (2015) co-registered a point cloud derived from UAV-based image sequences to LiDAR data over urban areas. Building outlines are detected in the images as well in order to colourize the LiDAR-based point cloud. The image orientation was performed with an average error of about 0.5 pixels, as reported for different test sites. This is a reasonable result, but still there is a need for existing LiDAR data and demands on the topography are similar to the ones listed in Förstner & Steffen (2007). This observation leaves us with the conclusion that, in order to have a generally applicable workflow for indirect orientation of UAV image blocks, still individual, highly accurate GCPs are needed, possibly in combination with a flight configuration which supports accurate self-calibration.

Other works analysed methods on how onboard GNSS and IMU can be integrated in the UAV workflow, in order to derive a better direct estimation of the position and attitude of the aircraft. Pfeifer et al. (2012) performed some preliminary tests using a low-cost onboard IMU and GNSS receiver and achieved a platform position accuracy better than 1 m. Eling et al. (2014) describe a prototype where RTK-GNSS, a second GNSS receiver for heading estimation, and a low cost IMU (MEMS-based) are integrated into a real-time position estimation approach. In the experiments the authors achieved a standard deviation of 1 cm to 2 cm in position and up to 1.5° in absolute angle measurements. Rehak et al. (2014) report about a similar system and obtained similar accuracy values, but the system was not capable of delivering results in

real-time. A different approach to direct sensor orientation is to use visual odometry, i.e. to employ stereo cameras for accurate (relative) attitude and position estimation. Schneider et al. (2014) combine such a method with RTK-GNSS to solve for the unknown position, rotation and scale within the mapping frame.

While the mentioned literature describes successful research prototypes, we can also observe that today UAV-vendors offer complete systems which integrate survey-grade RTK-GNSS localization on board the UAV. For instance, the Topcon B110 board is used in the Mavinci Sirius Pro, and the Sensefly Ebee RTK (MAVinci 2015, SenseFly SA 2015). Research showed that with this RTK-GNSS board it is possible in principle to assign to each camera exposure a position estimation in the range of 2 cm – 3 cm accuracy, i.e. much better than a standard DGPS solution (Bäumker et al. 2013). By now many more UAV-system vendors offer RTK-GNSS-enabled systems. However, in 2014, when the experiments for this paper were conducted, only the Mavinci system was available.

Within the bundle adjustment the RTK-GNSS observations assigned to each image would not only help to solve for the exterior image orientation in the given mapping frame, but also mitigate block deformation effects. Although the aforementioned research papers proved the positive influence of those direct observations onto the bundle block adjustment, a systematic analysis of commercially available systems has still not been carried out to our knowledge. The use of commercial systems has the advantage that experiments can be reproduced and have a larger relevance for practical applications.

3 Details on the RTK-supported Workflow

Many factors influence the accuracy of the position which is assigned to an image taken during the UAV flight. As the GNSS-RTK board can deliver an absolute position at 2 cm – 3 cm error level, the goal must be to minimize the remaining error coming from uncertainties of the relative alignment of the sensors on board of the UAV and data processing. The following components play an important role in this respect: calibration of offset from camera projection centre to antenna phase centre (boresight alignment), attitude of plane during exposure time, time synchronization, and last but not least a method to identify blunders during bundle adjustment.

As our dataset is from the Mavinci Sirius Pro system, we give details about the workflow implemented by this provider. The calibration of offsets from the camera projection centre to the GNSS antenna in the plane coordinate system is done during the manufacturing of the UAV, and cannot be repeated by the end user. In addition to the offset which assumes a horizontally positioned airplane, the attitude (yaw,

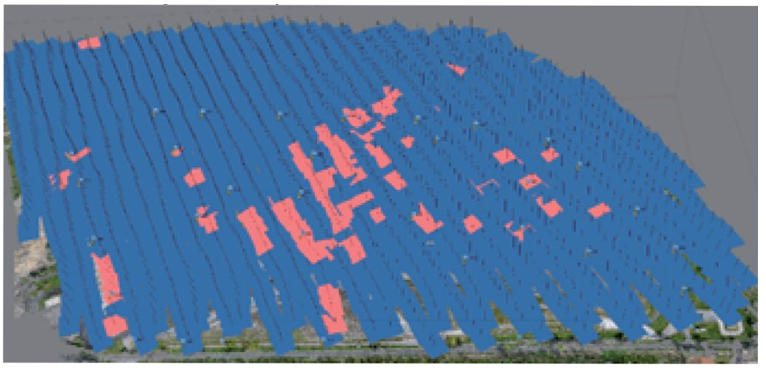

Fig. 1: Example block with images coloured according to the weights of the respective GNSS observations in the bundle adjustment: blue: estimated GNSS position accepted, position introduced with original weight; red: estimated absolute camera position with low weight in the bundle adjustment.

pitch, roll) is needed for each point in time to accurately correct for the lever arm offset. To this end, a MEMS-based INS sensor is used. For this task, but also to relate the correct exposure time to GNSS time, synchronization of all critical events is indispensable. Absolute positions, obtained from combined GNSS and IMU observations, are delivered at 100 Hz. Without interpolation of the positions this frequency would already lead to an error of up to 20 cm, depending on the flight speed. An additional uncertainty emerges from the fact that end-user cameras very often just work according to a rolling shutter principle, i.e. an optimal triggering needs to take into account the time delay occurring here. A permanent link from the ground control unit needs to be available in order to provide the UAV with the RTK-GNSS information and enable a real-time computation of the position and attitude parameters.

The last major issue concerns the actual absolute positioning accuracy of each single position observation assigned to the individual camera shots. In an iterative procedure outliers are identified. In case of the Mavinci system this iterative bundle adjustment is implemented in the Photoscan software package (Agisoft 2015). Initially all position parameters are included in the adjustment as observations with a pre-defined standard deviation of 2 cm in the horizontal plane and 3 cm in height. Detailed information on the workflow implemented in the software is not available. However, it can be assumed that after bundle adjustment the positional residuals are analysed and for all images showing large differences, the weight is decreased (i.e. the standard deviation increased) and the bundle adjustment is repeated. This process is iterated until the residuals of all remaining images with high weight are below a predefined threshold. In this way not only errors from the RTK solution (for instance caused by non-solved phase ambiguities) are taken into account, but in general also uncertainties originating from the entire calibration and correction process. In Fig. 1 an example image block is shown, indicating by colour for which image the provided position parameters are considered as being accurate (blue). Mostly the projection centre coordinates are introduced into the adjustment; IMU-based observations only play a minor role within the workflow because of lower quality. As automatically extracted points support tying images, this way in which GNSS-RTK measurements are included might be called partially integrated sensor orientation (Jacobsen 2004).

As far as the source of reference information for the realization of the RTK-solution is concerned, the vendors advise to set up a temporary reference station close to or in the area of interest in order to achieve a high accuracy.

4 Datasets

Two UAV datasets were acquired in early 2014. While area 1 (stockpile) is characterized by large height variations and sandy/rocky terrain, in area 2 (Zollern) we find several buildings in a largely flat terrain. Both datasets reflect usual application areas for fixed-wing UAV projects.

Area 1 (stockpile): Data acquisition took place in April 2014. The area is close to the German city of Duisburg, covers 1100 × 600 m^2, and the height difference between the highest and the lowest point equals 50 m. The employed Mavinci Sirius Pro UAV, which is equipped with the mentioned 2-frequency GNSS receiver board, including RTK capabilities, was programmed to deliver a forward overlap of 85%, and a sidelap of 65% at 105 m average flight height. The Panasonic LumixGX1-Pancake14mm-PRO camera took in total 1900 images, at an average GSD of 2.7 cm. In addition to the North-South flight realized in the described pattern, a smaller block, covering 20% of the area, was captured in a West-East direction at 75 m average height, refer to Fig. 2. A temporary GNSS reference station was installed within the area.

Area 2 (Zollern): This dataset was acquired in the framework of the ISPRS scientific initiative *ISPRS Benchmark For Multi-Platform Photogrammetry* (Nex et al. 2015) in May 2014. The test site covers an area of 500 × 350 m^2 and contains mostly historic buildings of a former coal mine, which today are used as museums. Except for two mine head tow-

ers no significant height variation is present. The flight parameters are similar to the ones used in area 1, refer to Fig. 3 for an overview. An important operational difference to area 1 is the access only to a regular Mavinci Sirius, without the GNSS-RTK option, hence this dataset was only used to analyse the impact of the cross flight pattern and GCP distribution. The camera used was of the same type as in area 1, but it was actually a different device.

Reference

For both areas well distributed 3D points were acquired. While in area 1 a standard RTK-GNSS system-based workflow was employed (35 points @ 3 cm standard deviation (3D)), in area 2 a static GNSS procedure was used to capture 34 points @ 2 cm standard deviation.

5 Experiments

Two different sets of experiment were carried out. The first one refers to the case where the UAV-based RTK-option is not used, but concentrates on the effect the cross-flight pattern has on the bundle block accuracy, and compares different GCP configurations. For this setup both datasets were employed. The second set of experiments additionally takes into account the RTK-option, while the remaining parameters are the same as in the first set. As the RTK-option was only available in area 1, this second part is only done with the stockpile dataset. Another important analysis concerns the impact that all different configurations have on self-calibration.

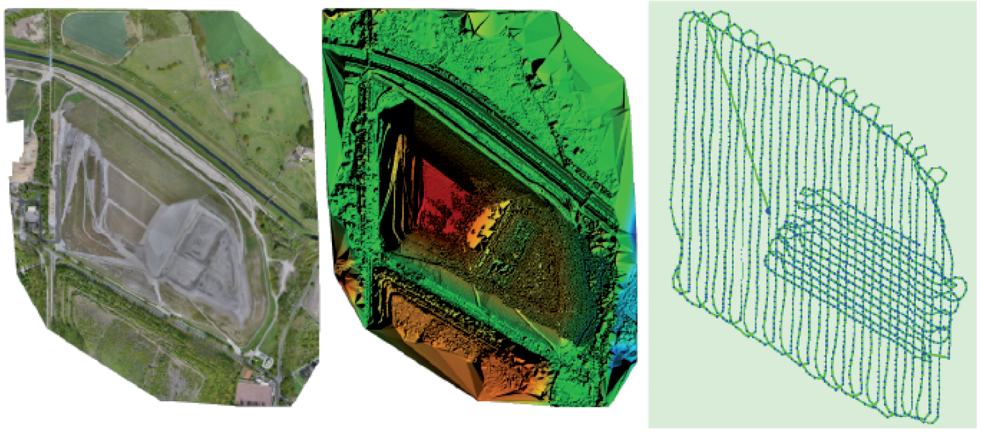

Fig. 2: Area 1, stockpile. Left: ortho image, middle: colour coded height model, right: flight plan.

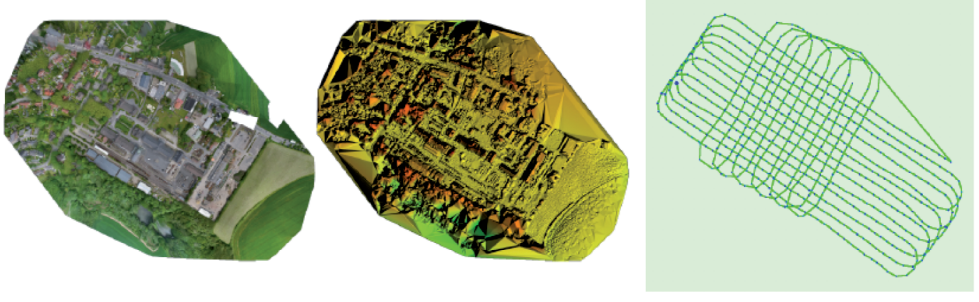

Fig. 3: Area 2, Zollern. Left: ortho image, middle: colour coded height model, right: flight plan.

5.1 *Cross Flight and GCP Distribution*

The first set of experiments does not make use of the RTK-option provided by the UAV system, but assumes a traditional setup, where only ground control points are provided. The main objective of this first analysis concerns two questions: a) how does the number and distribution of GCP influence the accuracy, and b) does the flight pattern with cross layout and two different heights have an influence of the final bundle accuracy? To brighten those questions in both test areas four different configurations are tested: to use only four 3D points as GCPs and to use about half of measured points as GCPs (17 and 18 in areas 1 and 2, respectively), and in addition those two setups were evaluated with and without the additional images from the cross flight. To analyse the accuracy, the X Y Z residuals at the remaining check points, i.e. all measured 3D points which have not been used for the bundle block adjustment, are used. In all setups an individual self-calibration, including estimation of lens distortion parameters, was conducted.

In Fig. 4 RMSE values are shown, separated into horizontal RMSE, vertical RMSE and the combined 3D RMSE. While the left half shows results from area 1 (stockpile), the right half refers to area 2 (Zollern). The respective left columns refer to experiments where the additional images from the cross flights are used, while the right columns show results from the main flight only. All RMSE values, also for the next section, are summarized in Tab. 1. In area 1 the cross flight pattern does not have a significant impact on the overall accuracy. We only observe a typical error reduction when more GCPs are used: The 3D RMSE decreases from more than 20 cm to about 8 cm. Especially the errors in height are large when only 4 GCPs are used: while the XY RMSE is below 5 cm, the RMSE in the Z component is about 20 cm, but it decreases down to 8 cm if 18 GCPs are used.

In area 2 the positive effect of the cross flight pattern onto the overall accuracy, but in particular onto the height accuracy, is obvious: already using only 4 GCPs in the cross pattern we obtain an overall 3D-RMSE of 3 cm, while it is almost 17 cm if only one flying height and -direction is used. The influence on the planimetric accuracy, however, is less significant. The reduction of the height error in the 4-GCP-case after using the additional images from the cross flight is large: the RMSE in Z is 16.5 cm without the use of the second image set and decreases to 2.4 cm when these images are used. In the next section we will elaborate

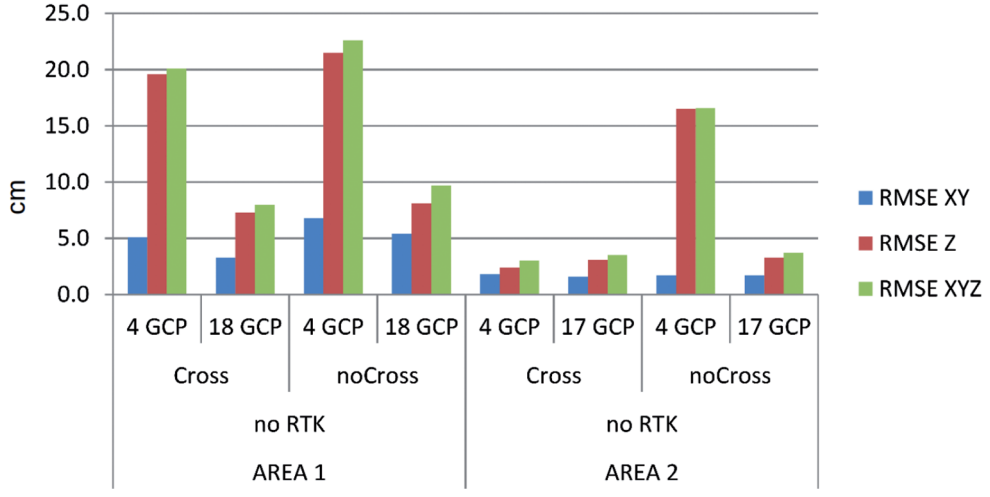

Fig. 4: RMSE of residuals at check points in area 1 and 2, with RTK disabled. Left columns with cross pattern used, right without. GCP: number of control points. In area 1, the number of check points is 31 if four and 17 if 18 GCPs are used. In area 2, the number of check points is 30 in case of four GCPs and 17 in case of 17 GCPs.

on the question whether these large Z-errors are caused by block deformation. When more GCPs are used, however, the difference between the two configurations concerning the use of the cross flight disappears. In both sets we reach the limit of our evaluation procedure: given that the ground control measurements have a standard deviation of 2 cm, and the theoretical accuracy of points measured in the UAV image block is at the GSD-level (σ = 2.5 cm), the largest one-σ error according to the error propagation rule we are able to detect is approximately 3.2 cm. Therefore, although the small RMSE values support a clear trend towards GSD-level accuracy, the numbers are not statistically significant.

5.2 *UAV-based RTK, Cross Flight and GCP Distribution*

The second set of experiments has been conducted with the RTK-option enabled, i.e. the RTK-GNSS data attached to each image was integrated into the bundle adjustment according to section 3. As the airplane equipped with RTK-option was only available in area 1, the second area is omitted here. In addition to the configurations analysed in section 5.1, we also assess the result achieved without GCPs. From a practical point of view this variant is interesting, e.g. for disaster scenarios where GCPs might not be available, or any other near-real time application.

In Fig. 5 the respective RMSE charts for the RTK-supported bundle block adjustments are shown. First we observe that, similar to the experiments above, the relative change from the left to the right part, i.e. the influence of the cross-flight, is not really substantial, but visible, especially in the horizontal components which show smaller RMSE values for the cross configuration. More insight is available when different GCP configurations are compared. Even without any use of ground control the block accuracy is at an error range of 6.8 cm 3D RMSE when the cross flight pattern is used, and in XY the RMSE is below 5 cm. A closer look at the spatial distribution will help to understand the situation. In Fig 6, the XY residuals (green) are plotted in combination with height residuals (blue). The red scale bar in the left corner equals 10 cm. The arrangement of points is according to the given UTM-grid with cropped leading digits to leave the axis legend readable. The left plot in that figure is from the configuration: 4 GCPs, cross-flight, noRTK, while the right plot shows the same configuration, except for the fact that the RTK-option was enabled. On purpose we show the 4-GCP-configuration in order to be able to examine typical block de-

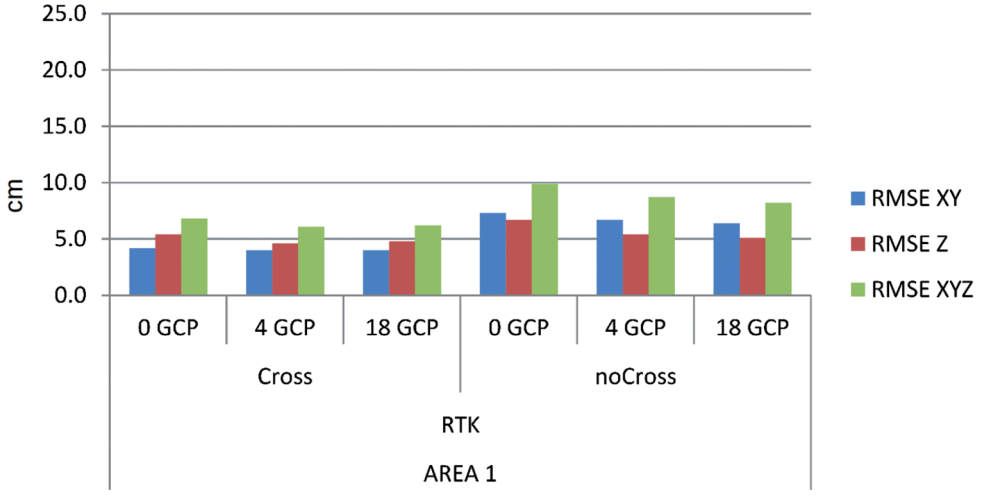

Fig. 5: RMSE of residuals at check points in area 1 with RTK enabled. Left column: cross-flight pattern used, right: no cross-flight pattern used. GCP: number of ground control points used. The number of check points is 35, 31, 17 if 0, 4 or 18 GCPs are used, respectively.

formation problems. The GCPs are distributed in the 4 corners of the block and in case no RTK is used (left plot in Fig. 6) the deformation, in particular towards the centre of the block is obvious. Closer to the GCPs those errors are reduced as expected. However, when we use the onboard RTK-option (right plot in Fig. 6), the deformation almost vanishes, and only in the southern part some Z-residuals increase to 8 cm.

Another important observation made in this second experiment show that the RMSE does not improve much with an increasing number of GCPs. For most configurations it is nearly constant. Here, once more we look at the error propagation. While for the UAV image block we assume a point measurement accuracy again of $\sigma = 2.5$ cm, the GCPs acquisition in area 1 was a bit more inaccurate compared to area 2, and we assume $\sigma = 3$ cm. These num-

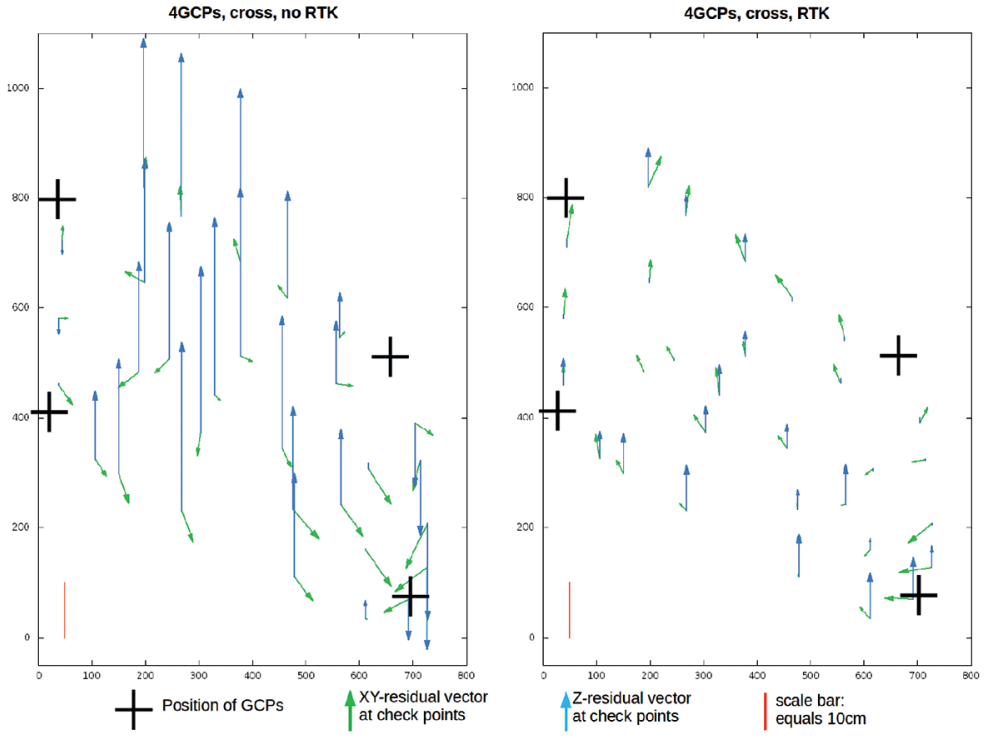

Fig. 6: Spatial plot of residuals, separated by XY- and Z-component. In both cases: use of 4 GCPs (black crosses), cross flight configuration, left: RTK-option disabled, right: RTK enabled.

Tab. 1: Horizontal / Z (3D) RMSE (cm) for all configurations as shown in Figs. 4, 5, and 6.

	No RTK (see Fig. 4)		RTK enabled (see Fig. 5)	
	Cross	**No Cross**	**Cross**	**No Cross**
Area 1, no GCPs	-----	----	4.2/5.4 (6.8)	7.3/6.7 (9.9)
Area 1, 4 GCPs	5.1/19.6 (20.1) (*Fig. 6, left*)	6.8/21.5 (22.6)	4.0/4.6 (6.1) (*Fig. 6, right*)	6.7/5.4 (8.7)
Area 1, 18 GCPs	3.3/7.3 (8.0)	5.4/8.1 (9.7)	4.0/4.8 (6.2)	6.4/5.1 (8.2)
Area 2, 4 GCPs	1.8/2.4 (3.0)	1.7/16.5 (16.6)	----	----
Area 2, 17 GCPs	1.6/3.1 (3.5)	1.7/3.3 (3.7)	----	----

bers lead to a combined standard deviation of approximately $\sigma = 4$ cm of the differences. Although we see a trend in the RMSE values towards a better accuracy when more GCPs are introduced, we cannot evaluate the quality more reliably.

Tab. 1 summarizes the results for all configurations: the left columns show the non-RTK solutions from the last section, while the right hand side shows the results from this section with enabled RTK.

5.3 *Impact on Self-Calibration*

In this section we further analyse the parameters of the interior orientation, i.e. focal length and principal point offset. Radial and tangential distortion parameters are estimated as well. In our experiments, however, they do not differ significantly for the different setups. In the projective camera model used in the employed software a scale factor for the pixel aspect is estimated as well, hence there are actually 4 parameters: px and py for the principal point offset with respect to image centre, and cx and cy which are actually composed as cx = mx*f, and cy = my*f, while mx and my are scale factors in column and row direction, respectively, and f the focal length. In Fig. 7 the values for px, py, cx, and cy are plotted for all experiments. The values cx and cy are differences to the approximations derived from EXIF headers. The upper diagram is for area 1, while the lower one refers to area 2.

While the principal point offset does only vary in a random pattern and with non-significant size, we can observe a certain trend for the focal length. The variations are small; they are 10 pixels at maximum for area 2, which is

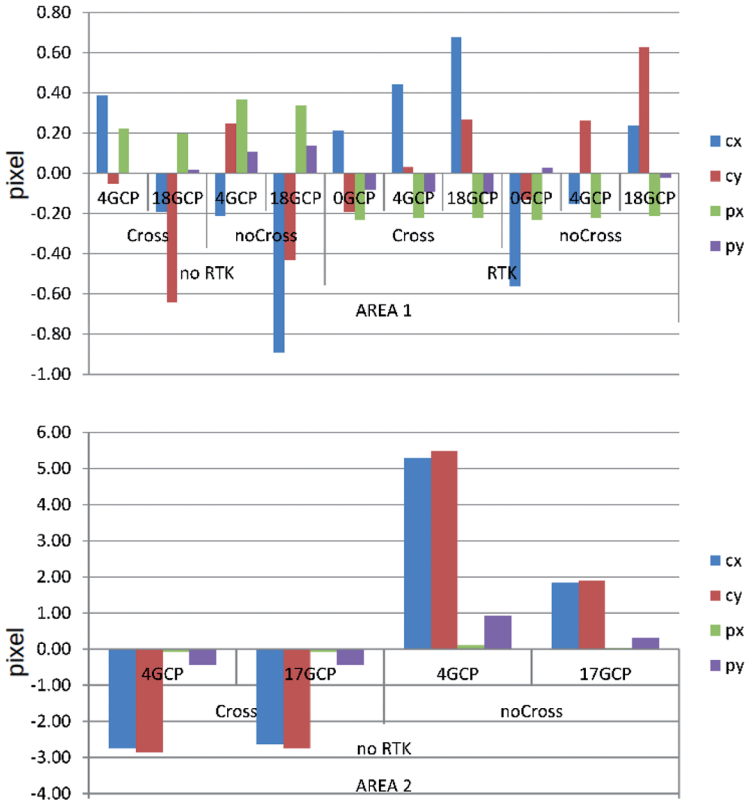

Fig. 7: Principal point offset (px, py) and focal length difference to initial values (cx,cy) for all experiments. Values in pixel. Note the different scaling in y.

equivalent to 35 µm. However, given the fact that in areas 1 and 2 the same type of camera was used, the variation in cx and cy is about ten times larger in area 2, compared to area 1. From this we might conclude that the actual estimation of the focal length is more uncertain in the flat area of Zeche Zollern (area 2), while in area 1 the flight configuration and surface variation helps to estimate a more stable set of parameters. Unfortunately, a deeper analysis of the statistical significance of differences observed in Fig. 7 or of correlations between was not possible, because Agisoft does not deliver precision values for the unknowns.

5.4 *Synchronization of Sensor Observations: Remaining Errors*

A very interesting observation can be made when estimated sensor locations from the GNSS-RTK approach are compared to the finally derived positions after GCP-supported bundle adjustment. The upper part of Fig. 8 shows a diagram which indicates the airplane speed during the operation, and in the lower part distances between GNSS-RTK-based and finally adjusted sensor positions are plotted. During the flight in area 1 it was quite windy and this is also reflected in the speed chart: UAV velocities vary from about 50 km/h to 95 km/h. The lower diagram indicates some

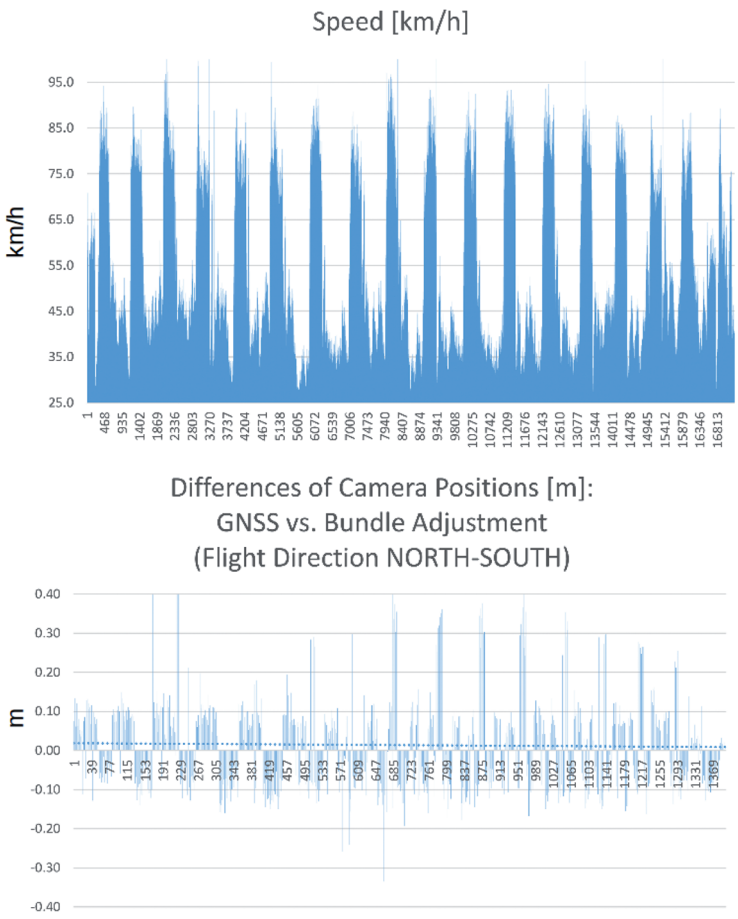

Fig. 8: Airplane speed as a function of time and difference in projection centre positions: GNSS-RTK solution vs. bundle adjustment using GCPs. Blue dotted line: average at 1.5 cm.

significant differences. The sign of the differences (offsets) alternates per strip, and the amplitude varies from 10 cm to 20 cm. The charts in Fig. 8 allow to argue that there is a certain correlation between the speed of the airplane and the observed offsets. Unfortunately, a rigorous analysis, e.g. by linear regression, is not possible because from the flight log the accurate time of image exposure cannot be retrieved. A possible explanation for the offsets can be a certain time gap between the position observation and the camera triggering. In order to roughly estimate the time gap a simple computation has been carried out: at a speed of about 55 km/h (15 m/sec) an average offset of 10 cm was registered, this means a delay of about 6 ms, while for the higher speed of 85 km/h (24 m/s) an average difference of 20 cm is visible, leading to a time gap of 8 ms. It must be noted that without more detailed sensor readings, e.g. also from the IMU and at sufficient frequency, a statistically sound analysis is not possible.

The absolute errors of 10 cm to 20 cm do not occur in the check point residuals, even if no GCPs are used (refer to Tab. 1 and Fig. 5). The 2D RMSE is about 4 cm. The explanation for this is the flight in regular strips and the change of heading of the airplane at the end of every strip. Thus, the absolute error averages out. Actually, the mean offset (see blue dotted line in lower chart of Fig. 8) is 1.5 cm.

6 Discussion, Conclusions and Outlook

Concerning the first objective of this research, which was to analyse the influence of a cross-flight pattern and the GCP distribution on the bundle block adjustment we saw a quite different behaviour in the two test areas. In area 1 the residuals at checkpoints, in case the images from the cross-flight were used, were of a similar size as in the case where only the images from the main flight were utilized. The main reason for this is probably that area 1 shows some natural height elevation changes, leading to fewer problems in self-calibration. This assumption is confirmed by the analysis of the internal orientation parameters: the variation of the focal length is negligible. However, the XY error is always a bit smaller when the second image set is used. Thus, we might conclude that the different flight directions contribute to a more accurate estimation of the principal point. Probably due to a lack of natural elevation differences in area 2, the positive effect the cross-flight pattern has onto the final accuracy is significant, first of all in the Z component. The relatively large variation of the calibrated focal length supports the assumption of an inaccurate self-calibration. When many GCPs are introduced into the bundle adjustment, the difference in RMSE between those two setups is not visible anymore: obviously the camera self-calibration improves or remaining errors are better compensated through the exterior orientation, respectively, when more GCPs are provided. Although the applied software does not provide statistic measures on the adjusted unknowns it is likely that the parameters of external and internal orientation are highly correlated. Thus, it is difficult to use self-calibration if the terrain is not undulated or cross-flight patterns at different altitudes are not possible. This might also influence the final accuracy. In those cases a well pre-calibrated (metric) camera should be used (Luhmann et al. 2015).

As far as the second aim of this paper is concerned, namely to quantify whether the influence of the integrated RTK-UAV workflow provides an enhancement on absolute image orientation accuracy, we can discuss some findings here as well. Because of the effects in conjunction with possibly less accurate 3D point measurements we cannot conclude on the absolute accuracy obtainable, however, we can make very important observations when we compare the different setups. Even if no GCPs are introduced, the accuracy in object space is better compared to the setup without the use of the RTK-UAV option, but with more GCPs enabled (the 3D RMSE is 1 cm smaller). From this, we can draw the conclusion that the absolute block orientation accuracy can be enhanced significantly by using the onboard RTK solution. Block deformation is a typical problem in UAV image blocks, especially when the block is not supported by well distributed GCPs. This observation was also made here, refer to Fig. 6, but the problem is mitigated considerably when using sup-

port through the RTK-option, at least in our experiments the block deformation was hardly visible in that case. Despite the competitive results obtained from the GNSS-RTK-supported solution we observed synchronization errors resulting in absolute positional offsets. In the regular image block these errors were obviously averaged out, but in less regular blocks or free flights those errors need to be considered.

From all these finding we can derive some important hints for the practice. First of all, if the terrain does not show much undulation we would advise to plan a cross-flight, at least in some parts. The inclusion of RTK-based image position observations into the UAV processing workflow turned out to have a very positive effect, in particular onto the height component. With our experiments we showed that even a UAV-RTK-only solution delivers results which are superior to the traditional completely indirect sensor orientation. In those cases, however, it is important to provide at least some check points with very high accuracy, e.g. as delivered through static GNSS, in order to be able to thoroughly validate the obtained results. This is especially important in the light of the detected remaining synchronization uncertainties.

In the future, we expect to see more RTK-supported UAV image processing hardware and processing pipelines. Typical applications fields like multi-temporal data acquisition (vegetation monitoring, building construction monitoring) would definitely benefit from the demonstrated accuracies that we obtained without the inclusion of ground control and that might be sufficient. UAV-based damage mapping is another field of interest (Vetrivel et al. 2015). In some areas like forests GCP acquisition might not be possible, and if data from previous epochs or old maps are to be combined with new images, accurate georeferencing is indispensable. One of the next steps would also include the integration of such a RTK-GNSS device plus INS like the Trimble BD 935 in a rotary wing platform, potentially directly mounted at the gimbal, or even at the camera (Trimble Inc. 2015). If it were possible to also approximate the attitude of the optical axis, in addition to a precise position, we could expect at least a faster and more efficient camera orientation. Alsadik et al. (2013) already showed that the knowledge of approximate camera locations and viewing direction could decrease processing time tremendously and at the same time increase the overall reliability.

Acknowledgements

The authors would like to acknowledge the provision of the datasets by ISPRS and EuroSDR, captured in the framework of the ISPRS scientific initiative 2014 and 2015, led by ISPRS ICWG I/Vb. We also thank the anonymous reviewers who gave very valuable feedback.

References

Agisoft, 2015: Agisoft Photoscan software. – http://www.agisoft.com (11.11.2015).

Alsadik, B., Gerke, M. & Vosselman, G., 2013: Automated camera network design for 3D modeling of cultural heritage objects. – Journal of Cultural Heritage **14** (6): 515–526; http://doi.org/10.1016/j.culher.2012.11.007.

Bäumker, M., Przybilla, H.-J. & Zurhorst, A., 2013: Enhancements in UAV Flight Control and Sensor Orientation. – The International Archives of the Photogrammetry, Remote Sensing and Spatial Information Sciences **XL–1/W2**: 33–38; http://doi.org/10.5194/isprsarchives-XL-1-W2-33-2013.

Cramer, M., 2001: Genauigkeitsuntersuchungen zur GPS/INS-Integration in der Aerophotogrammetrie. – PhD Dissertation, Deutsche Geodätische Kommission, Reihe C, 537, 120 p.

Colomina, I. & Molina, P., 2014: Unmanned aerial systems for photogrammetry and remote sensing: A review. – ISPRS Journal of Photogrammetry and Remote Sensing, **92** (0): 79–97; http://doi.org/10.1016/j.isprsjprs. 2014.02.013.

Eling, C., Klingbeil, L., Wieland, M. & Kuhlmann, H., 2014: Direct georeferencing of micro aerial vehicles – system design, system calibration and first evaluation tests. – PFG – Photogrammetrie, Fernerkundung, Geoinformation **4:** 227–237.

Förstner, W. & Steffen, R., 2007: Online Geocoding and Evaluation of Large Scale Imagery without GPS. – Photogrammetric Week 2007: 243–253, Herbert Wichmann.

Jacobsen, K., 2004: Direct Integrated Sensor Orientation – Pros and Cons. – The International Archives of the Photogrammetry, Remote Sensing and Spatial Information Sciences **XXXV/W3:** 829–835.

Luhmann, T., Fraser, C. & Maas, H.-G., 2015: Sensor modelling and camera calibration for close-range photogrammetry. – ISPRS Journal of Photogrammetry and Remote Sensing, in press, 10 p.; http://dx.doi.org/10.1016/j.isprsjprs.2015.10.006.

MAVinci, 2015: SIRIUS PRO Surveying UAS. – http://www.mavinci.de/en/siriuspro (11.8.2015).

Nex, F., Gerke, M., Remondino, F., Przybilla, H.-J., Bäumker, M. & Zurhorst, A., 2015: ISPRS benchmark for multi – platform photogrammetry. – ISPRS Annals of the Photogrammetry, Remote Sensing and Spatial Information Science **II–3/W4:** 135–142; http://doi.org/10.5194/isprsannals-II-3-W4-135-2015.

Nex, F. & Remondino, F., 2014: UAV for 3D mapping applications: a review. – Applied Geomatics **6** (1): 1–15; http://doi.org/10.1007/s12518-013-0120-x.

Nocerino, E., Menna, F., Remondino, F. & Saleri, R., 2013: Accuracy and Bock Deformation Analysis in Automatic UAV and Terrestrial Photogrammetry – Lessons learnt. – ISPRS Annals of the Photogrammetry, Remote Sensing and Spatial Information Science **II-5/W1:** 203–208; http://doi.org/10.5194/isprsannals-II-5-W1-203-2013.

Pfeifer, N., Glira, P. & Briese, C., 2012: Direct Georeferencing With on Board Navigation Components of Light Weight UAV Platforms. – The International Archives of the Photogrammetry, Remote Sensing and Spatial Information Sciences **XXXIX/W7:** 487–492.

Przybilla, H.-J., Reuber, C., Bäumker, M. & Gerke, M., 2015: Untersuchungen zur Genauigkeitssteigerung von UAV-Bildflügen. – 35. Wissenschaftlich-Technische Jahrestagung der DGPF **24:** 45–54.

Rehak, M., Mabillard, R. & J. Skaloud, J., 2014: A micro aerial vehicle with precise position and attitude sensors. – PFG – Photogrammetrie, Fernerkundung, Geoinformation **4:** 239–251.

Rumpler, M., Daftry, S., Tscharf, A., Prettenthaler, R., Hoppe, C., Mayer, G. & Bischof, H., 2014: Automated End-to-End Workflow for Precise and Geo-accurate Reconstructions using Fiducial Markers. – ISPRS Annals of the Photogrammetry, Remote Sensing and Spatial Information Science **II–3:** 135–142; http://doi.org/10.5194/isprsannals-II-3-135-2014.

Schneider, J., Läbe, T. & Förstner, W., 2014: Real-Time Bundle Adjustment with an Omnidirectional Multi-Camera System and GPS. – 4th International Conference on Machine Control & Guidance: 98–103.

SenseFly SA, 2015: eBee RTK. – https://www.sensefly.com/drones/ebee-rtk.html (11.8.2015).

Trimble Inc., 2015: Trimble bd935-ins. – http://intech.trimble.com/oem_gnss/receiver_boards/trimble_bd935-ins (11.8.2015).

Vetrivel, A., Gerke, M., Kerle, N. & Vosselman, G., 2015: Identification of damage in buildings based on gaps in 3D point clouds from very high resolution oblique airborne images. – ISPRS Journal of Photogrammetry and Remote Sensing **105:** 61–78.

Watts, A.C., Ambrosia, V.G. & Hinkley, E.A., 2012: Unmanned Aircraft Systems in Remote Sensing and Scientific Research: Classification and Considerations of Use. – Remote Sensing **4** (12): 1671–1692; http://doi.org/10.3390/rs4061671.

Yang, B. & Chen, C., 2015: Automatic registration of UAV-borne sequent images and LiDAR data. – ISPRS Journal of Photogrammetry and Remote Sensing **101:** 262–274; http://doi.org/10.1016/j.isprsjprs.2014.12.025.

Addresses of the authors:

Dr.-Ing. Markus Gerke, University of Twente, Faculty of Geo-Information Science and Earth Observation – ITC, Department of Earth Observation Science, Hengelosestraat 99, Enschede, The Netherlands. Tel.: +31-53-4874-522, e-mail: m.gerke@utwente.nl

Prof. Dr.-Ing. Heinz-Jürgen Przybilla, Bochum University of Applied Sciences, Department of Geodesy, Lennershofstr. 140, 44801 Bochum, Germany. Tel.: +49-234-32-10517, e-mail: heinz-juergen.przybilla@hs-bochum.de

Manuskript eingereicht: August 2015
Angenommen: Dezember 2015

PFG 2016 / 1, 031 – 043
Stuttgart, February 2016

Article

Evaluation Criteria for Recent LoD Proposals for CityGML Buildings

Marc-O. Löwner, Braunschweig & Gerhard Gröger, Bonn

Keywords: Virtual 3D city models, semantical data models, CityGML, Level of Detail, evaluation criteria

Summary: The Level of Detail (LoD) concept is an essential part of the Open Geospatial Consortium standard CityGML and of 3D city models in general. New applications such as indoor navigation and energy performance estimation ask for a revision of the current CityGML 2.0 LoD concept. Currently, new approaches are discussed that need to be evaluated. Here, new evaluation criteria for the assessment of recent Level of Detail concepts in the field of semantical 3D city models are developed. They cover richness of aspects, completeness of the concept, completeness of models in a particular LoD, avoidance of inconsistent models, freedom of interpretation, and feasibility and complexity of transformation from CityGML 2.0 into the proposed concept. These criteria represent an added value because user defined LoD profiles of the new CityGML version 3.0 LoD concept are likely and therefore need to be evaluated. Applying the developed criteria, we evaluate the most current proposals on the further development of the CityGML 2.0 LoD concept.

Zusammenfassung: *Kriterien zur Bewertung aktueller Vorschläge für Gebäude-LoD in CityGML.* Der Detaillierungsgrad (Level of Detail, LoD) stellt ein wesentliches Konzept von CityGML, dem internationalen Standard des Open Geospatial Consortiums für semantische 3D-Stadtmodelle, dar. Neue Anwendungsfelder wie die Innenraumnavigation oder die Energiebedarfsanalyse erfordern allerdings eine Überarbeitung der in CityGML 2.0 definierten Konzepte und haben bereits eine Folge von Verbesserungsvorschlägen nach sich gezogen. Hier werden neue Evaluationskriterien zur Bewertung aktueller LoD-Konzepte von semantischen 3D-Stadtmodellen vorgestellt. Diese Kriterien umfassen die Reichhaltigkeit der Aspekte, die Vollständigkeit des Konzeptes, die Vollständigkeit der Modelle innerhalb eines LoD, die Vermeidung inkonsistenter Modelle, die Interpretationsfreiheit sowie die Möglichkeit und Komplexität der Transformation von CityGML 2.0 in das vorgeschlagene Konzept. Die Definition solcher Kriterien ist wichtig, weil für CityGML 3.0 die Möglichkeit diskutiert wird, Profile der LoD Definition zuzulassen. Mittels der neu entwickelten Kriterien werden die aktuellen Verbesserungsvorschläge des LoD Konzeptes bewertet.

1 Introduction

Virtual 3D city models represent single buildings, city quarters, whole cities and even regions for applications such as noise propagation simulation and mapping (Czerwinski et al. 2007), fine dust distribution modelling (Ghassoun et al. 2015), urban and telecommunication planning (Köninger & Bartel 1998, Knapp & Coors 2008), or real-time simulations for emergency driving training (Randt et al. 2007). Some application areas such as emergency management (Zlatanova & Li 2008) or indoor navigation (Becker et al. 2009) even require information of the building's interior on a city level. These models may vary with regard to geometrical and semantical complexity and to the degree of deviation from the corresponding real world objects. Complexity levels then are the result of specific data acqui-

www.schweizerbart.de
DOI: 10.1127/pfg/2016/0282 1432-8364/16/0282 $ 3.25

sition processes or they may be used to assess the suitability of data for specific applications.

The Open Geospatial Consortium (OGC) *CityGML* standard (Gröger et al. 2012, Gröger & Plümer 2012) for the representation of semantically enriched 3D city models has introduced a Level of Detail (LoD) concept in order to support different applications of 3D city models. It does not only cover the geometrical detail level, but also the semantical one, i.e. the richness of feature types modelled. The current LoD concept of CityGML 2.0 provides five discrete levels of detail. Its definition is widely accepted in the scientific community (e.g. Boguslawski et al. 2011, Quinn et al. 2009, Iwaszczuk & Stilla 2010, Fan et al. 2009, Götzelmann et al. 2009, Guerke et al. 2009). The term "*LoDx model*", $x \in \{0, 1, 2, 3, 4\}$, is frequently used to address the complexity of existing city models and their suitability for specific applications. However, some deficiencies have been identified, which hamper the use of CityGML for important applications. In particular, indoor objects are coupled with the highest LoD in CityGML 2.0, implying highly complex semantics and geometry. Hence, applications requiring only coarse indoor models or indoor models in combination with a coarse exterior are not supported. Further, there are no multiple LoD for indoor objects in CityGML 2.0 (e.g. coarse or highly detailed 3D representations, or 2D footprints) which are required for indoor navigation (Domínguez et al. 2011, Hagedorn et al. 2009). In addition, the explicit representation of windows in an outer wall of a building is only possible in LoD3, which requires an accurate geometrical representation of the building façade. To estimate a building's energy demand, however, explicit information on the area covered by windows is needed, whereas a very coarse representation of the façade's geometry is sufficient (Dalla Costa et al. 2011).

To overcome these deficiencies, modifications or extension of the LoD concept have been proposed (Boeters et al. 2015, Biljecki et al. 2013, Biljecki et al. 2014, Benner et al. 2013, Löwner et al. 2013, Nagel 2014). Until today, none of these proposals or possible combinations of their single aspects have been evaluated to be the best LoD concept for 3D city models in a comparative approach. Assessment criteria for the comparison of LoD approaches which are relevant for 3D city model collectors, providers and users are still missing.

Currently, there is a discussion in the CityGML community whether the fixed and standardized geometrical representation for a particular LoD, e.g. *LoD1Solid* or *LoD2MultiSurface* for buildings, should be replaced by a more flexible and generic model where each *CityObject* can be represented by any geometry type. According to this framework, restricting *profiles* may be defined for particular *CityObjects* including one official profile in the CityGML Specification. Thus, evaluation criteria become even more important.

Here, the assessment criteria *richness of aspects*, *completeness of the concept*, *completeness of models in a particular LoD*, *avoidance of inconsistent models*, as well as *feasibility and complexity of transformation from CityGML 2.0* for the evaluation of LoD concepts are introduced and applied to the most recent approaches. The term 'aspect' denotes a component of the data model that is relevant for the LoD concept, for example geometry, semantics, appearance, or topology. However, since no formal definitions are given, we see this contribution as a beginning of a discussion about requirements on LoD concepts.

In section 2 we give an overview on recent LoD concepts for semantical 3D city models focussing mainly on the CityGML Building model. The criteria, which are the base of the comparison, are introduced in section 3. The evaluation and comparison of the approaches introduced in section 2 is presented in section 4. We will end with conclusions and an outlook.

2 Recent Level of Detail Concepts for Semantical Building Models

This section gives an overview over three recent LoD concepts for semantical 3D building models that are related to the further development of CityGML. For a detailed description of the CityGML 2.0 LoD concept reference is made to Löwner et al. (2013), Gröger et al. (2012), and Gröger & Plümer (2012). A more

general overview of LoD concepts for semantic 3D city models can be found in Benner et al. (2013).

2.1 *The Benner Approach*

The Benner approach (named after its main contributor Joachim Benner) is directly related to the further development of the CityGML standard (Benner et al. 2013, Löwner et al. 2013). It exhibits two modifications: First, there is an explicit separation between a geometrical and a semantical LoD. Second, the current LoD4 has been mapped to four LoD for the interior. Hence, a building is partitioned into an exterior and an interior, both with one or more explicit LoD of geometrical and semantical aspects.

For geometry, the Benner approach supports four different representations (LoD0 to LoD3) for all top-level features of the CityGML building model, whether they represent the building's exterior shell (*Building*, *BuildingPart*, …) or interior components (*Room*, …). Benner et al. (2013) identify the semantical structuring and classification as an important criterion for virtual 3D city models. They define four different *Semantical Levels* (S0 – S3) for the *Building* model's top level features. As for the Geometrical LoD, the Semantical Levels of exterior shell and rooms may be different. If a building refers to more than one room, all corresponding *Room* features must have the same Semantical Level.

Since this extended concept allows for building models representing the exterior building shell as well as interior rooms in different geometrical and semantical LoD with only some restrictions on acceptable combinations, new labels have been defined that extend the existing CityGML 2.0 labels. They are a combination of geometrical and semantical labels where the latter is put in brackets, e.g. LoD2.1(S2.0) for a building with an exterior shell in LoD2 together with interior Objects in LoD1 where *Building*, *BoundarySurfaces* and *BuildingInstallations* for the exterior and *Rooms* for the interior are semantically classified.

2.2 *The Biljecki Approach*

The Biljecki approach (Biljecki et al. 2013) does not only focus on CityGML, but also on proprietary approaches for 3D city models that are developed by commercial companies. An LoD is defined as a quality measure with regard to a specific application. This measure is related to a variety of aspects including richness of feature types, attribute richness, complexity of geometrical details, appearance quality, and positional accuracy. Separate hierarchies for geometry and semantics are proposed, which have to be defined by users. Further, it is proposed to define constraints for each LoD, which assure its consistency. An example is a constraint that prevents interior geometries without exterior ones.

A modification of this approach with a similar set of six aspects is presented in Biljecki et al. (2014). These aspects are applied to the exterior and the interior of features. They span a space of six dimensions, and an LoD is defined as a vector of six values or ranges of values. Only *consistent series* of LoD0, …, LoD*n* are considered, which have to be monotonic in each aspect. This means that from one LoD(*i*) to the next LoD(*i*+1) in the sequence, the values of the six aspects increase or remain unchanged, but never decrease. Hence, there is a total order on the LoD in a series that than allows for the comparison of two LoD. As an example for the implementation of the framework, a series LoD0 to LoD9 is defined. The main aspects are *existence of features*, *geometrical correspondence between model and reality*, and *resolution of the appearance*. These 10 LoD are roughly a refinement of the LoD0 to LoD4 in CityGML 2.0. The concept is implemented as an extension of CityGML (formally, an Application Domain Extension).

2.3 *The Nagel Approach*

The Nagel approach (named after Claus Nagel who was the first to propose this concept) is built on practical experience and directly related to the further development of CityGML 2.0 (Löwner et al. 2015, Nagel 2014). It needs just two definitions. First, every city object has a spatial representation in

every LoD that refines its spatial representation in higher LoD. That means secondly, that there is no restriction on the usage of any feature type in an LoD. Thus, even feature types that have been limited to CityGML 2.0 LoD4, e.g. a *CeilingSurface,* can be used in any lower LoD. In this approach, LoD0 stands for planar representations and LoD1 for prismatic blocks model representations of a feature. Further, LoD2 models represent a generalised shape of a *CityObject* whereas LoD3 represents it in its highest geometrical complexity.

In order to improve flexibility, a distinction is made between volumetric geographic features and *BoundarySurfaces*. An *AbstractBuilding*, for instance, is then modelled with zero to two instances of a *GM_MultiSurface* in LoD0, representing the footprint or the edges of a roof. For the representation in LoD1 to LoD3 it is modelled as a *GM_MultiSurface* or as a *GM_Solid*, respectively. An *AbstractBoundarySurface*, which might be possible in all four LoD is represented by a *GM_MultiCurve* in LoD0 and zero to one *GM_MultiSurfaces* in LoD1 to LoD3. Here, the curve representation stands for the footprint as a spatial abstraction of that wall surface.

The proposed concept stands out with its clear and short definition. By allowing all feature types being modelled in LoD0 to LoD3 an explicit LoD for interior features becomes obsolete.

3 Definition of Criteria for the Comparison of recent LoD Concepts

In order to compare the LoD concepts, six criteria are introduced: *richness of aspects*, *completeness of the concept*, *completeness of models in a particular LoD*, *avoidance of inconsistent models*, *freedom of interpretation*, and *feasibility and complexity of transformation from CityGML 2.0.*

Richness of aspects

A Level of Detail concept for semantical 3D city models may define more than just the aspect of geometrical similarity of the model and the real world feature. In contrast to computer graphics, it also may cover the semantical LoD, i.e. the richness of feature types such as wall surfaces, installations, or building parts represented in the model. In addition, other aspects of a model can be considered, e.g. its appearance, attribute data and so forth. However, a useful LoD concept should cover more than just geometry or, at least should be extensible to other aspects like semantic or appearance. An increasing complexity of the concept itself and the labelling of instance documents are inextricably linked to this criterion.

Completeness of the concept

Completeness of the concept is the degree to which the concept allows for the representation of data. A concept is complete if all datasets can be represented. The more restrictions apply, the lesser is the completeness. Even models which may be considered as inconsistent might lead to a higher degree of completeness. An example is a 3D dataset with coarse interior objects (blocks model rooms) with highly detailed outer shell penetrated by the room geometries. Such a model is well suited for energy applications, where a rough estimation of the indoor volume is sufficient, but detailed roof structures with dormers are required for solar panel placement planning. In addition, this criterion plays a role for legacy data. Such datasets often violate consistency rules of data models or LoD concepts, e.g. thresholds for geometrical accuracy, topological inconsistencies, or missing semantical classifications, but might be valuable since there are no other datasets available.

Since inconsistent models may increase the completeness of the concept, this criterion is inverse to the criterion ‘avoidance of inconsistent models’.

This criterion is crucial for users of 3D city models, which have to check whether the data needed for an intended application can be represented by a particular LoD concept. Likewise, for data collectors it is important to check whether captured data can be represented.

Completeness of models in a particular LoD

This criterion is the degree to which completeness of instant models in a single LoD is forced by the concept. A model is complete in a particular LoD if the concept states that

all objects or their parts specified in the particular LoD and existent in the real world are represented in the dataset. One precondition for completeness is the LoD being defined for principal objects, e.g. buildings, primarily for those, which have to represented completely. The LoD of the subordinated features (boundary surfaces, installations, etc.) is determined by the LoD of the principal objects. For example, if a concept provides boundary surfaces and installations in LoD2 and defines that a 'LoD2 building' has an complete outer shell and is completely bounded by boundary surfaces, the LoD2 model of this concept is complete. Likewise, if an 'LoD3 building' requires a complete outer shell with boundary surfaces and openings as feature types, it is complete. If the LoD is defined for each feature type separately, there are no dependencies and, thus, the completeness of models in an LoD is low. This concept would allow representing a single opening or single furniture without any buildings or rooms.

This criterion refers to the rules of an LoD concept and to the degree to which the concept demands completeness. Hence, this criterion can be evaluated by inspecting the concept. It is another issue outside the scope of this discussion whether a particular dataset is complete with regard to an LoD specification (an issue of quality principles evaluation procedures, c.f. ISO 19157:2013). This completeness typically can be assured based on reference data only.

This criterion is of interest for applications which require complete models, for example to assess the energy loss of a building, which rely on models where each opening (door or window) is represented as a feature in the building model.

Avoidance of inconsistent models

This criterion determines whether the LoD specification contains a sufficient explicit or implicit set of integrity rules to assure that the model instances are meaningful. The risk to produce inconsistent models can be avoided by declaring an appropriate LoD concept for virtual 3D buildings. Weak definitions may lead to inconsistent model instances even if the modeller follows all rules and restrictions defined. Inconsistency may occur on the geometrical level if interior structures penetrate the exterior shell due to different interior and exterior LoD. Semantically, inconsistency may occur if more semantical information is allowed to be attached to a coarse and undifferentiated geometry. Therefore, this assessment criterion results also from the completeness of concept.

Freedom of interpretation

An LoD concept may restrict the freedom of interpretation of the modeller. Therefore, it should be clearly defined and avoid ambiguity to result in comparable results when applying modelling rules. Clarity of definition is particularly of interest for the relationship between vendor and customer. Both parties should agree whether a concrete instance model is suited for a specific application and whether the model contains all the data to fulfil the user's demands. Further, a precisely defined Level of Detail concept aiming at improving description of the dataset can lead to a faster and more robust development of application software, e.g. with respect to support switching between different LoD. This also entails a comprehensible and unambiguous labelling of different LoD. Informative value of the label is an essential element when restricting the freedom of interpretation. Thus, the expression of a clearly defined LoD concept leads to unambiguous instance models.

For collectors and providers of data, however, an ambiguously defined model has the advantage of less effort to build up a 3D city model. In addition, legacy models might fit better to an ambiguously defined model. Hence, the scope of such models is significantly wider.

Feasibility and complexity of transformation from CityGML 2.0

Since 2008 many companies, federal surveying agencies and municipalities, responsible for the representation and provision of their 3D city models use CityGML, worldwide. Hence, the required effort to transform these models to a newer version of CityGML with a modified LoD concept (if this transformation is feasible at all) is an important criterion. If models conforming to the new LoD concept are syntactically and semantically compatible with

CityGML 2.0, the complexity is zero. If there is a simple one-to-one mapping between the names of the elements in the model, the complexity is very low. The complexity is high if complex structural or geometrical transformations or classification processes are required to transfer datasets to the new concept.

This criterion is related to the freedom of interpretation. If it is higher in the source than in the target concept, mapping requires the often complex classification of the vague one. For example, if geometry details of the source concept are vaguely defined but mandatory in the target concept, the geometry has to be classified (for example, as LoD1, 2 or 3 geometries) in order to assign the level in the target concept.

4 Comparison of four recent LoD Concepts

Based on the criteria introduced in section 3, we now evaluate the discussed LoD approaches and compare them. An overview of the evaluation results is given in Tab. 1. The order of evaluation is the same for all criteria: 1) CityGML 2.0, 2) Benner approach, 3) Biljecki approach, (example LoD0 – LoD9 instancing the Biljecki framework will be examined additionally), and, 4) Nagel approach.

4.1 *Richness of Aspects*

The CityGML 2.0 LoD concept enables the representation of a *CityObject* in different geometrical LoD and provides a refined semantical description with ascending LoD. However, geometric and semantic complexity of a building model is strictly coupled. In LoD0 and LoD1 no further decomposition of a *Building* or *BuildingPart* into other feature classes or semantic classification is possible. LoD2 represents the prototypic roof shape of a building, thematic ground, wall and roof surfaces as well as installations, such as balconies and dormers. LoD3 as the most detailed level for the outer shape allows for the semantical representation of openings. LoD4 adds interior structures like rooms, furniture, interior installations. While a certain LoD enforces a specific geometric representation, the increase of semantic complexity is only optional. Therefore, it cannot be stated that a semantical LoD is entirely independent.

Regarding geometry, the Benner approach supports four different representations for all top-level features of the CityGML building model regardless whether they represent the building's exterior shell (*Building*, *BuildingPart*, etc.) or interior components. Next to the aspect of geometry Benner et al. (2013) define four different *Semantical Levels* (S0 – S3) for

Tab. 1: Overview of the evaluation of LoD concepts according to the criteria developed in section 3. Ratings range from '– –' (not fulfilled at all) to '++' (completely fulfilled). '/' means that the criterion is not applicable.

	CityGML 2.0	Benner	Biljecki (framework)	Biljecki (LoD0 – 9)	Nagel
Richness of aspects	±	+	+ +	+	–
Completeness of the concept	±	+	±	±	+ +
Completeness of Models in an LoD	±	+ +	+ +	+ +	– –
Avoidance of inconsistent models	+ +	– –	+ +	+ +	– –
Freedom of interpretation	+ +	±	– –	– –	+ +
Feasibility and complexity of transformation from CityGML 2.0	/	+	– –	– –	+ +

the *Building* model's top level features. As for the Geometrical LoD, the Semantical Levels of exterior shell and rooms may be different. If a building refers to more than one room, all corresponding *Room* features must have the same Semantical Level.

In comparison to the CityGML 2.0 LoD concept the Benner approach reveals a higher richness of aspects including a graduation of interior details, the independent representation of different semantical LoD for exterior and interior and an independent semantical Level of Detail for both, the interior and exterior building.

The Biljecki approach defines a very rich LoD concept involving six aspects, which consider semantics (features, attributes), geometry (accuracy, dimensionality), appearance and the relation between geometry and semantics. The exterior and the interior of features are considered separately. Combinations of these aspects are restricted by the concept of series of LoD, which forces an increase of the values of the particular aspects if the LoD number increases. The proposed implementation of the approach (LoD0 – LoD9) uses only a subset of the aspects of the general framework (feature complexity, dimensionality, and appearance). Nevertheless, the richness of both concepts is significantly higher than the richness of all other proposals.

The Nagel approach allows all *CityObjects* to be modelled in every LoD, geometrically. Consequently, an extra LoD for interior feature types, the CityGML 2.0 LoD4, becomes unnecessary. These results in four LoD from LoD0 for surface representations of real-world features, e.g. the ground surface of a building, to LoD3 for the most detailed representation of modelled features. For instance a boundary surface, which can only be modelled from LoD2 in the CityGML 2.0 LoD concept, can be represented as a curve in LoD0 that represents the 'surface of a wall' in the real word. Therefore, the Nagel approach is more flexible than the CityGML 2.0 LoD concept.

No semantical LoD is introduced by the Nagel approach. However, since the CityGML 2.0 LoD concept restricts the usage of some feature types in lower LoD, e.g. a boundary surface in LoD0, it is argued, that the Nagel approach allows for semantically richer models, at least in lower LoD. A floor plan may be considered as an example. Because all feature types can be used to represent the 2D representation of a story, i.e. *IntBuildingInstallation*, *InteriorWallSurface*, *Door*, *Window*, etc. the floor plan is semantically rich and can be queried for wall surfaces, doors, columns, and so forth.

4.2 *Completeness of the LoD Concept*

The completeness of the LoD concept is low for CityGML 2.0, since there are a lot of restrictions between the two aspects of geometry and semantics. First, indoor objects can only be represented in the most detailed LoD. Coarse room representations, which are relevant for energy applications, for example, are out of scope of the concept. Second, semantical richness and complexity of the geometry are coupled. Not all combinations of geometrical and semantical complexity are supported. Hence, datasets which are suitable or required for some applications cannot be represented by CityGML. For example, openings cannot be represented in combination with coarser outer shell of a building. Also rooms cannot be combined with such a coarse outer representation. On the other hand, incomplete instance models in an LoD (see next criterion) can be represented by CityGML 2.0, for example a single opening without any building or wall. Hence, the completeness of the LoD concept is high for such 'incomplete' instance models.

In the Benner approach rooms can be represented in any geometrical detail level, and combinations of indoor objects and the outer building shell are possible. A geometrical detail level can be combined with an arbitrary semantical level, due to the separation into geometrical and semantical LoD. Only a few restrictions remain such that boundary surfaces, openings and building installations cannot be geometrically represented in LoD0 or LoD1.

In the Biljecki approach, the exterior and the interior are separated. Hence, each combination of indoor and outdoor LoD can be represented. However, the completeness is restricted by the monotonicity condition, stating that the value of an aspect cannot decrease in

a higher LoD. Hence, geometry and semantics are coupled, as it is the case in CityGML 2.0. The concept is more restricted than the Benner approach, which allows for combinations of geometric and semantical aspects, despite the restrictions mentioned.

The concrete implementation of the Biljecki concept by defining LoD1 to LoD9 is significantly more restricted than the general framework, since exterior and interior are coupled. Coarse indoor objects cannot be represented with a fine exterior. Hence, the completeness is comparable to the completeness of the CityGML 2.0 LoD concept.

The Nagel approach is based on geometry only and has no restrictions at all. Hence, the completeness of the LoD concept is maximal.

With regard to new application areas which initially were the motivation for a modified LoD concept, both, the Nagel and the Benner approach meet the requirements. The Nagel approach is not restricted at all while in the Benner approach, the two aspects geometry and semantics are independent and can be arbitrarily combined. In the general Biljecki approach, the combination of aspects is restricted by the monotonicity condition. Since exterior and interior are separated, more applications are supported. In the concrete implementation, however, interior and exterior are coupled. Hence, neither energy applications (coarse interior / fine grained exterior) nor indoor applications (2D interior objects) are possible.

4.3 *Completeness of Models in a particular LoD*

In CityGML 2.0, a LoD is defined for principal objects such as buildings and it is implied that the corresponding models are complete in that LoD. However, this is stated only narratively in the specification, but is not defined in the mandatory part: neither the UML diagram, nor the XML schemas or the conformance requirements state this explicitly. Hence, the completeness of models in a particular LoD is low.

In the Benner approach, an LoD is also defined for principal objects. The geometrical as well as the semantical label explicitly state the content of such an object. This holds for the geometry and for the semantical content. The latter is explicitly defined by a list of feature types which have to be present in the model. Hence, the models are complete with regard to these labels.

The general framework of Biljecki provides an aspect ‘Feature Complexity’, which is explicitly defined as ‘fineness of geometry with respect to the real world’. As a straightforward way to denote this, the minimal length of objects is mentioned; if this condition is fulfilled, the object has to be represented in the model. Hence, the models are complete, at least for objects which are larger than this minimal dimension. Since the concrete implementation of the framework contains the aspect ‘Feature Complexity’, it is complete as well.

The Nagel approach defines LoD for each feature separately and independently. If a building feature, for example, is labelled as LoD3, no statement on the occurrence of subordinate feature types are made. Hence, completeness of models in a particular LoD is low.

4.4 *Avoidance of Inconsistent Models*

The CityGML 2.0 LoD concept for buildings is very straight-lined because the LoD attribute is obliquely devoted to the building object itself. As a result, higher detailed buildings consist of an optional superset of features describing the building of the particular lower Level of Detail. In addition, the list of features that represent a building in a specific LoD is defined, thus preventing the assignment of more semantical information to a coarse and undifferentiated geometry. Further, the highest geometrical representation for both, the exterior shell and the interior is required in LoD4 so that interior structures cannot penetrate the exterior shell. Thus, a violation of semantics and geometry is virtually impossible.

The Benner approach determines the complete LoD of a building by the combination of Geometric LoD and Semantical LoD. Therefore they define feasible combinations. Geometric LoD0 models can only be combined with Semantical Level 0, while geometric LoD1, LoD2 and LoD3 models are allowed to represent four variants with increasing semantical complexity. These restrictions result in 13

feasible combinations of Geometrical LoD and Semantical LoD for the building exterior and interior and make inconsistent models of geometric and semantic combination impossible.

The Benner approach distinguishes between exterior and an interior Level of Details. Thus, geometrical problems might occur if the LoD of the geometrical detail level of the exterior and the interior are not identical. For instance, if rooms have a detailed geometry, but the exterior is coarse, fitting problems are likely to happen. Either the room geometry penetrates the exterior shell, or empty spaces inside the building are not covered by rooms. Vice versa, if rooms have a coarse geometry, but the exterior shell is fine-grained, the room geometry might penetrate the exterior shell (rf. Fig. 15 in Benner et al. 2013).

In the general framework of Biljecki, there is a strict separation between indoor and outdoor objects. Hence, inconsistent models might also happen here. However, it is stated in Biljecki et al. (2014) that 'the interior is constrained with the exterior'. However, it is not completely clear what this exactly means and whether those inconsistencies are prevented. In the concrete implementation LoD0 to LoD9 of the Biljecki framework, the geometry detail increases for indoor and outdoor in a similar way and are comparable to the CityGML 2.0 concept. Hence, violations between indoor and outdoor objects are not possible.

The Nagel approach defines LoD not for an entire building, but for every particular *CityObject* with no restriction on how a composed building should be modelled using *CityObjects* in different LoD. Thus, this proposal might lead to inconsistent models as already identified for the Benner approach. Moreover, the label for a certain LoD does not belong to an entire building any longer, but to its composing feature types.

4.5 *Freedom of Interpretation*

The CityGML 2.0 specification provides definitions of the particular LoD in terms of geometry and semantics that are very vague with respect to geometrical complexity. Semantics of an LoD is defined in terms of feature classes for buildings and its parts, but only a maximal set of such feature types is provided. Hence, the semantical richness is optional.

In addition to a geometrical representation, an LoD3 model might have boundary surfaces, openings, and installations, which again might have boundary surfaces. However, it is not strictly required that such features are present in an LoD3 building representation. Therefore, all of the following models would be qualified as LoD3: building geometry only, building geometry and thematic surfaces, thematic surfaces only, building geometry, thematic surfaces and openings as well as thematic surfaces and openings. Since *BuildingParts* and *BuildingInstallations* are other optional feature types, which both can be combined with these five options, the number of different LoD3 models is at least 20. Here, only semantical variability is considered. If additionally geometrical aspects are taken into account, this number increases significantly.

Consider a simple blocks model with thematic boundary surfaces and openings as an example for a problematic LoD classification. The question is how to classify such a model. Classification as LoD1 or LoD2 is impossible, since these schemata do not provide openings. Technically, it is possible to qualify such a model as LoD3. Admittedly, this violates the definition of LoD3, which 'denotes architectural models with detailed wall and roof structures' (Gröger et al. 2012). To sum up, it can be said that freedom of interpretation is high for the CityGML 2.0 approach.

The Benner approach defines a compact nomenclature incorporating exterior and interior Geometrical and Semantical Levels, which specializes the CityGML 2.0 LoD indicators and results in a substantially higher informative value of the label. It indicates the geometrical modeling style and the semantic modeling depth of a *Building* or *BuildingPart*, consistently extending the CityGML LoD notation. Ambiguities are almost impossible and the freedom of interpretation is low.

The aspects in the Biljecki approach are defined very precisely. The criterion 'Presence of city objects and elements' defines the feature types which have to be present in a particular LoD. The 'Feature Complexity' allows specifing concrete minimal dimensions of fea-

tures, and 'Attribute data' a concrete list of attributes. Hence, the freedom of interpretation is low. This also holds true for the concrete implementation of the framework. For each LoD (0 to 9), concrete values for the feature complexity such as minimal size of objects is given, e.g. 10 m in LoD0 for building blocks or 10 cm in LoD9.

In the Nagel approach, only one criterion, the detail level of geometry, is used. However, this criterion is not defined precisely, but only intuitively by giving figures as examples. Hence, the freedom of interpretation is supposed to be high.

4.6 *Feasibility and Complexity of Transformation from CityGML 2.0*

The Benner and the Nagel approach have in common that LoD4 has been replaced by LoD3 for interior and exterior objects. The additional LoD4 outer geometry has deliberately been introduced into CityGML in order to provide the possibility to adapt the outer shell to the interior objects, in particular to fit the openings of rooms. Although the LoD4 outer geometry may differ from the LoD3 outer geometry, only one representation (LoD3) is provided by both, the Benner and the Nagel approach. Hence, there might be a loss of information when transforming CityGML 2.0 datasets containing LoD3 and LoD4 into either concepts.

A general problem when transforming datasets from CityGML 2.0 is the vagueness of definitions with respect to geometry. Even if it contradicts the common understanding of LoD3, a coarse block can be used as a LoD3 representation without breaking syntactical rules or conformance requirements of the CityGML 2.0 concept.

Apart from the aforementioned problems, the mapping from CityGML 2.0 into the Benner approach can be easily performed. LoD0 is mapped to LoD0(S0) while LoD1 is mapped to LoD1(S1). Further, LoD2 is mapped to LoD2(S2), if the conditions of LoD2 (semantics) are completely fulfilled. If the semantic conditions of S1 respectively S0 are fulfilled, LoD2 is mapped to LoD2(S1) or LoD2(S0), respectively. LoD3 is mapped to LoD3(S3), if the conditions of LoD3 are completely fulfilled. If openings are not represented, it is mapped to LoD3(S2). If *BoundarySurfaces* are not represented, it is mapped to LoD3(S1). Finally, LoD4 is mapped to LoD3.3(S3.3), if the conditions of LoD4 are completely fulfilled. However, it is mapped to LoD3.x(S3.y), if the conditions for semantical completeness are fulfilled only partially. The value for x has already been defined in the mapping for LoD3, whereas y is set to 2 if openings are not represented completely, y is set to 1 if in addition the interior building installations and the building furniture are missing. Finally, y is set to 0 if boundary surfaces are not present. The fulfillment of the semantical conditions can easily be checked by scanning the dataset.

The Biljecki approach provides strict, precisely defined requirements for the geometry. In order to check whether for instance a CityGML 2.0 LoD3 model satisfies the minimal dimension of the corresponding LoD of Biljecki, it is not sufficient to consider the datasets only. Instead, the corresponding real world objects have to be inspected, which is very elaborate and expensive. For the transformation into the concept of Biljecki, first the aspects on which the LoD concept is based on have to be compared. The geometry aspect of CityGML corresponds most likely to the 'Feature Complexity'. Whether semantics is modelled or not in a particular LoD is covered by the 'Presence of CityObjects and Elements' aspect. Hence, the CityGML 2.0 aspects are a subset of the Biljecki aspects and, in general, datasets can be transformed. However, the problem of vague geometry definition in CityGML 2.0 versus a very precise definition of the Biljecki approach remains. Due to this, the transformation is very elaborate.

For the example LoD 0 to 9, the mapping is as follows: For LoD0, there is no counterpart; at least not for buildings (there are no areal representations for buildings). LoD1 corresponds to LoD1, LoD2 to LoD3 (since there is no interior in LoD2, the interior representation in LoD3 is empty). LoD3 is represented as LoD8 (again without interior) and finally LoD4 is represented as LoD9.

The transformation of CityGML 2.0 models according to the Nagel approach is straightforward: The LoD of each feature can be de-

rived immediately from its geometry properties. Only a simple syntactical transformation is required. Hence, it is the LoD concept with the smallest transformation complexity.

5 Summary and Discussion

This paper evaluates and compares different proposal for the revision of the CityGML 2.0 LoD concept. Therefore, new evaluation criteria are developed reflecting the needs that are relevant for stakeholders of 3D city models. These criteria cover such questions as: Can all 3D city building models be represented by the concept? To which degree are inconsistent models prohibited, as they nevertheless might be adequate for some applications? Can user rely on models to be complete in terms of all parts defined in that LoD (likely to be a high burden for data collectors)? Are all aspects, which might be relevant for users, e.g. geometry, semantics, and appearance reflected by the concept? How flexible and vague are the definitions? Vaguely defined concepts widen the scope of models and alleviate data collection. Strictly defined concepts are more reliable for users. Is it feasible to transform current models into the new concept and what are the transformation costs? However, the evaluation procedure can not formally be defined, since we consider concepts and their rules and specifications. The evaluation whether or to which degree a concept fulfils a specific criterion is performed by discursively inspecting the specifications of the concepts.

Four current and relevant proposals from academia and the commercial sector as well as the CityGML 2.0 concept are discussed and compared in relation to these criteria. The degree to which the criteria are fulfilled is very heterogeneous among the approaches. The Nagel approach is very flexible without any constraints, but allows for models with few properties users can rely on. The Benner approach indicates the semantic content of models in a reliable way, and is nearly as flexible as the Nagel approach. Far more precise and mandatory is the Biljecki approach, which, however, has some of the restrictions of the current CityGML 2.0 model. The costs for transforming CityGML 2.0 models to this concept are high.

It is expected that the evaluation presented here will be very valuable for the definition of the LoD profiles of the new LoD concept of CityGML 3.0. The group which will develop the official LoD profile can profit from the result, as well as users which will define own LoD profiles, in order to accommodate for their applications of 3D city models. This approach is innovative, since up to now, evaluation criteria for LoD concepts have not been developed and no systematic evaluation and comparison of current LoD approaches were possible.

References

Becker, T., Nagel, C. & Kolbe, T.H., 2009: A Multilayered Space-Event Model for Navigation in Indoor Spaces. – Lee, J. & Zlatanova, S. (eds.): 3D Geo-Information Sciences, Lecture Notes in Geoinformation and Cartography: 61–77, Springer, Berlin, Heidelberg.

Benner, J., Geiger, A., Gröger, G., Häfele, K.H. & Löwner, M.O., 2013: Enhanced LoD Concepts for Virtual 3D City Models. – ISPRS Annals of the Photogrammetry, Remote Sensing and Spatial Information Sciences **II-2/W1:** 51–61.

Biljecki, F., Zhao, J., Stoter, J. & Ledoux, H., 2013: Revisiting the concept of level of detail in 3D City Modelling. – ISPRS Annals of the Photogrammetry, Remote Sensing and Spatial Information Sciences **II-2/W1:** 63–74.

Biljecki, F., Ledoux, H., Stoter, J. & Zhao, J., 2014: Formalisation of the level of detail in 3D city modeling. – Computers, Environment and Urban Systems **48:** 1–15.

Boeters, R., Arroyo Ohori, K., Biljecki, F. & Zlatanova, S., 2015: Automatically enhancing CityGML LoD2 models with a corresponding indoor geometry. – International Journal of Geographical information Science **29** (12): 2248–2268; http://doi.org/10.1080/13658816.2015.1072201.

Boguslawski, P., Gold, C. & Ledoux, H., 2011: Modeling and analyzing 3D buildings with a primal/dual data structure. – ISPRS Journal of Photogrammetry and Remote Sensing **66** (2): 188–197.

Czerwinski, A., Sandmann, S., Stöcker-Meier, E. & Plümer, L., 2007: Sustainable SDI for EU noise mapping in NRW – best practice for INSPIRE. – International Journal for Spatial Data Infrastructure Research **2** (1): 90–111.

Dalla Costa, S., Roccatello, E. & Rumor, M., 2011: A CityGML 3D Geodatabase for Buildings Energy Efficiency. – International Archives of the Photogrammetry, Remote Sensing and Spatial Information Sciences **XXXVIII-4/C21:** 19–24.

Domínguez, B., García, Á. & Feito, F.R., 2011: Semantic and topological representation of building indoors: an overview. – The Joint ISPRS Workshop on 3D City Modelling & Applications and the 6th 3D GeoInfo Conference, Wuhan, China.

Fan, H., Meng, L. & Jahnke, M., 2009: Generalization of 3D Buildings Modelled by CityGML. – Sester, M. et al. (eds.): Advances in GIScience. – 12th AGILE Conference, Lecture Notes in Geoinformation and Cartography: 387–405, Springer, Berlin, Heidelberg.

Ghassoun, Y., Löwner, M.O. & Weber, S., 2015: Exploring the Benefits of 3D city Models in the Field of Urban Particles Distribution Modelling – a Comparison of Model Results. – Breunig, M. et al. (eds.): 3D Geoinformation Science, the Selected Papers of the 3D GeoInfo 2014. – Lecture Notes in Geoinformation and Cartography: 193–205, Springer.

Götzelmann, T., Guerke, R., Brenner, C. & Sester, M., 2009: Terrain-Dependent Aggregation of 3D City Models. – ISPRS-Workshop on quality, scale and analysis aspects of city models. – International Archives of the Photogrammetry, Remote Sensing and Spatial Information Sciences **XXXVIII-2/W11**, Lund, Sweden.

Gröger, G., Kolbe, T.H., Nagel, C. & Häfele, K.H. (eds.), 2012: OGC City Geography Markup Language (CityGML), Encoding Standard, Version 2.0.0., Open Geospatial Consortium. – OGC Doc. No. 12-019, Open Geospatial Consortium, 2012.

Gröger, G. & Plümer, L., 2012: CityGML – Interoperable semantic 3D City Models. – ISPRS Journal of Photogrammetry and Remote Sensing **71:** 12–33.

Guerke, R., Brenner, C. & Sester, M., 2009: Generalization of 3D City Models as a Service. – ISPRS-Workshop on quality, scale and analysis aspects of city models, International Archives of the Photogrammetry, Remote Sensing and Spatial Information Sciences, **XXXVIII-2/W11**, Lund, Sweden.

Hagedorn, B., Trapp, M., Glander, T. & Döllner, J., 2009: Towards an Indoor Level-of-Detail Model for Route Visualization. – MDM '09, Tenth International Conference on Mobile Data Management: Systems, Services and Middleware: 692–697, IEEE Computer Society, Piscataway, NJ, USA.

Iwaszczuk, D. & Stilla, U., 2010: A Concept for the Assignment of Textures to Partially occluded Faces of 3D City Models stored in CityGML. – Kolbe, T.H. et al. (eds.): 5th ISPRS International 3D GeoInfo Conference, Germany. – International Archives of the Photogrammetry, Remote Sensing and Spatial Information Sciences **XXXVIII-4/W15:** 57–62, Berlin.

Knapp, S. & Coors, V., 2008: The use of eParticipation in public participation: The VEPs example. – Coors, V. et al. (eds.): Urban and regional data management. – Urban Data Management Society Symposium 2007 (UDMS Annual 2007), BALKEMA-proceedings and monographs in engineering, water and earth sciences: 93–104, Taylor & Francis, London, UK.

Köninger, A. & Bartel, S., 1998: 3D-GIS for Urban Purposes. – Geoinformatica **2** (2): 79–103.

Löwner, M.O., Benner, J., Gröger, G. & Häfele, K.H., 2013: New Concepts for Structuring 3D City models – an extended Level of Detail concept for CityGML Buildings. – Murgante, B. et al. (eds.): 13th International Conference on Computational Science and Its Applications, Part **III, LNCS 7973:** 466–480, Springer, Berlin.

Löwner, M.O., Benner, J. & Gröger, G., 2015: Aktuelle Trends in der Entwicklung von CityGML3.0. – Seyfert, E. et al. (eds.): Geoinformationen öffnen das Tor zur Welt, 34. Wissenschaftlich-Technische Jahrestagung der DGPF, Tagungsband **23**, Hamburg.

Nagel, C., 2014: Proposal for a revision of the CityGML LOD concept. – Presentation at the 5th Meeting of OGC Working Package 3 for the revision of the LoD concept for CityGML 3.0, 20. 10. 2014, Bonn; https://github.com/opengeospatial/CityGML-3.0/blob/master/WP%2003%20Resources/Meetings/1st/WP03_2014_07_09_Nagel_Proposal_for_a_Revision-of-the-LOD-Concept.pdf (1.11.2015).

Quinn, J.A., Smart, P.D. & Jones, C.B., 2009: 3D city registration and enrichment. – ISPRS-Workshop on quality, scale and analysis aspects of city models. – International Archives of the Photogrammetry, Remote Sensing and Spatial Information Sciences **XXXVIII-2/W11**, Lund, Sweden.

Randt, B., Bildstein, F. & Kolbe, T.H., 2007: Use of Virtual 3D Landscapes for Emergency Driver Training. – 2007 IMAGE Conference, Scottsdale, AZ, USA.

Zlatanova, S. & Li, J. (eds.), 2008: Geospatial information technology for emergency response. – ISPRS book series, Taylor & Francis, London, UK.

Addresses of the Authors

Prof. Dr.-Ing. Marc-Oliver Löwner, Institute of Geodesy and Photogrammetry, Technische Universität Braunschweig, Pockelsstraße 3, 38106 Braunschweig, Germany, e-mail: m-o.loewner@tu-bs.de

Priv.-Doz. Dr. rer. nat. Gerhard Gröger, CPA Software GmbH, Auf dem Seidenberg 3a, 53721 Siegburg, Germany, e-mail: groeger@uni-bonn.de

Manuskript eingereicht: August 2014
Angenommen: Oktober 2015

Berichte von Veranstaltungen

ISPRS Konferenz „Photogrammetric Image Analysis“ (PIA15) und „High Resolution Earth Imaging for Geospatial Information“ (HRIGI15), 25. – 27. März 2015 in München

Mit großem Erfolg wurden die bekannten ISPRS Konferenzen *Photogrammetric Image Analysis* (PIA) und *High Resolution Earth Imaging for Geospatial Information* (HRIGI) zum ersten Mal im Rahmen einer gemeinsamen Veranstaltung durchgeführt. Unter dem Dach der Technischen Universität München und dem Vorsitz von Uwe Stilla und Christian Heipke konnten vom 25. bis zum 27. März insgesamt über 180 Wissenschaftler, Experten und Anwender aus 86 verschiedenen Einrichtungen in 27 Ländern aktuelle Forschungsergebnisse vorstellen und diskutieren (Abb. 1).

Die gemeinsame Ausrichtung von PIA und HRIGI ermöglichte einen gelungenen Austausch zwischen den Themengebieten „Semantik“ und „Geometrie“. Entsprechend der starken thematischen Auffächerung dieser fusionierten Konferenz beteiligten sich daran sieben ISPRS Arbeitsgruppen, namentlich: „LiDAR, SAR and Optical Sensors for Airborne and Spaceborne Platforms“ (WG I/2), „Geometric and Radiometric Modeling of Optical Airborne and Spaceborne Sensors“ (WG I/4), „Orientation and Surface Reconstruction“ (WG III/1), „3D Scene Analysis“ (WG III/4), „Methods for the Update and Verification of Geospatial Databases“ (WG IV/1), „DEM Generation and Surface Deformation Monitoring from SAR Data“ (WG VII/2), und „Pattern Analysis in Remote Sensing“ (ICWG III/VII).

Die inhaltliche Basis der Konferenz lieferten 36 Fachvorträge in 10 Sitzungen und 46 Posterpräsentationen in 3 interaktiven Blöcken. Hinzu kamen zwei Grundsatzreferate (Keynote), gehalten von Tomas Pajdla von der Czech Technical University in Prag mit dem Titel „Solving Minimal Problems For 3D Reconstruction From Images“ (Abb. 2a), sowie von Richard Bamler vom Deutschen Zentrum für Luft und Raumfahrt (DLR) über das Thema „TerraSAR-X, TanDEM-X and Beyond“ (Abb. 2b). Die Vorträge wurden in thematisch sortierten Vortragsblöcken mit den Titeln „Conditional Random Fields“, „Terrestrial“, „Forest Monitoring“, „Geometry“, „Synthetic Aperture Radar“, „Digital Elevation Models“, „Image Analysis“ und „Buildings“ sowie einem Vortragsblock der Industrie „From Sensors to Solutions“ abgehalten. Die Vortragsblöcke wurden ohne zeitliche Überschneidung (single track) und im Wechsel mit den Präsentationen der Poster abgehalten.

Im Zuge der Konferenzeröffnung gratulierten Uwe Stilla und Christian Heipke neun

Abb. 1: Teilnehmer der Konferenz PIA15+HRIGI15 Konferenz aus Sicht eines RPAS.

DOI: 10.1127/pfg/2016/0286 1432-8364/16/0286 $ 1.75

(a)

(b)

Abb. 2: Keynote speakers (a) Tomas Pajdla und (b) Richard Bamler.

(a)

(b)

Abb. 3: a) Christian Heipke (5. v. l.) und Uwe Stilla (1. v. r.) mit den Empfängern der Anreisestipendien vergeben durch TIF – The ISPRS Foundation und b) Best Poster award, Gunho Sohn (Mitte).

Teilnehmern zum Erhalt von Reisestipendien, vergeben durch „The ISPRS Foundation“ (TIF) (Abb. 3a). Den „Best Paper Award“ erhielten Javier A. Montoya-Zegarra, Jan Dirk Wegner, Lúbor Ladický und Konrad Schindler von der Eidgenössischen Technischen Hochschule in Zürich (ETH) für ihren Beitrag mit dem Titel: „Semantic Segmentation of Aerial Images in Urban Areas with Class-Specific Higher-Order Cliques“. Den Preis für das beste Poster erhielten Mozhdeh Shahbazi, Gunho Sohn, Jérôme Théau und Patrick Ménard, deren Posterpräsentation mit dem Titel: „Robust Sparse Matching and Motion Estimation using Genetic Algorithms“ an drei verschiedenen Institutionen in Kanada entstand (Abb. 3b).

Die sehr gut konzipierte Gesamtgliederung des Programms ermöglichte eine angenehme Abwechslung aus Informationsvermittlung und anregender Diskussion. Hierfür sorgten nicht zuletzt zwei abendliche Veranstaltungen bei der die Konferenzteilnehmer in angenehmer Atmosphäre bis in die späten Abendstunden diskutieren und neue Kontakte knüpfen konnten. Neben der Einführungsfeier (Icebreaker) im Vorhoelzer Forum, einem kleinem Salon umrandet von großen Balkonen mit einem freien Blick über die Dächer Münchens, war vor allem der abendliche Empfang im Münchener Künstlerhaus ein besonderes Ereignis (Abb. 4). Hier hatten die Veranstalter zu einem gemütlichen Abend bei sehr guter Verpflegung und dem bekanntlich schmackhaften bayerischen Bier in historischen Räumlichkeiten geladen, die von der Firma Hexagon unterstützt wurde. Das Vortragsprogramm sowie eine Fotogalerie finden sich unter http://www.pia15.tum.de

(a)

(b)

Abb. 4: a) Alphornbläser und b) Abendessen im Münchener Künstlerhaus.

Den Organisatoren ist eine international vernetzende und hochinformative Konferenz gelungen, die in jeder Hinsicht erfreute. Hierfür gebührt den hauptverantwortlichen Uwe Stilla, Christian Heipke und Ludwig Hoegner sowie zahlreichen weiteren Mitgestaltern und Helfern vor Ort großer Dank seitens aller Konferenzteilnehmer.

Damian Bargiel, Darmstadt

Hochschulnachrichten

Karlsruher Institut für Technologie

Dissertation von Andreas Schenk

Herr Dipl.-Ing. Andreas Schenk wurde am 28.1.2015 an der Fakultät für Bauingenieur-, Geo- und Umweltwissenschaften des Karlsruher Instituts für Technologie (KIT) mit der Arbeit *PS-Interferometrie in urbanen Räumen – Optimierte Schätzung von Oberflächenbewegungen mittels Multi-SBAS-Verfahren* zum Dr.-Ing. promoviert.

1. Referent: Prof. Dr.-Ing. habil. Bernhard Heck, KIT
2. Referent: Prof. Dr.-Ing. habil. Stefan Hinz, KIT

Kurzfassung:
Satellitenaufnahmen von SAR-Sensoren können mittels Radar-Interferometrie ausgewertet werden, um differentielle Verschiebungen der Erdoberfläche im mm-Bereich zu bestimmen. Die Persistent Scatterer Interferometrie (PSI) ist eine Methode der SAR-Interferometrie, bei der Stapel von Interferogrammen systematisch nach Rückstreupunkten durchsucht werden, die über längere Zeit stabil sind und daher als natürliche geodätische Messpunkte zur kontinuierlichen Beobachtung von Oberflächenbewegungen dienen. Für diese Punkte wird im Rahmen der Parameterschätzung der PSI unter anderem die exakte Position sowie die Punktverschiebung bestimmt. Mit der Entwicklung hochauflösender SAR-Sensoren erschließt sich auch die Beobachtung von lokalen und kleinräumigen komplexen Oberflächendeformationen sowie daraus resultierenden Gebäudebewegungen als potentielles Anwendungsgebiet der PSI.

Lokale Bodenbewegungen können anthropogene oder natürliche Ursachen haben. Mit der intensiven Bewirtschaftung des Untergrundes können sie insbesondere auch in urbanen Räumen durch den Menschen induziert werden. Die im Zusammenhang mit aufquellenden Gipskeuperschichten beobachteten Hebungsgebiete sind beispielhaft für solche lokalen Deformationsereignisse. Insbesondere in städtischen Gebieten müssen sie möglichst flächendeckend und kontinuierlich beobachtet werden. Die bisherigen Methoden der PSI sind für die Bewegungsbeobachtung solcher komplexen Deformationsgebiete nur bedingt geeignet, da sie auf der Annahme einer räumlich lokal stetigen Oberflächenbewegung basieren. Neben einer fehlerhaften Parameterschätzung werden bei der Anwendung in solchen Deformationsgebieten deutlich weniger PS-Punkte identifiziert.

In der Arbeit wurde der Frage nachgegangen, inwiefern die bestehenden PSI-Ansätze adaptiert werden können, um sie für die Untersuchung lokaler Deformationsphänomene zuverlässig anwenden zu können. Dabei werden die Methoden der Small Baseline Interferometrie berücksichtigt, um durch eine separate Bestimmung der Modellparameter auf multiplen Interferogrammstapeln die Effizienz und Robustheit der Parameterschätzung zu erhöhen und gleichzeitig eine zuverlässige Auswahl der PS-Punkte auch bei großen Bewegungsraten zu ermöglichen. Für die auf der Periodogrammschätzung basierende Parameterbestimmung werden zwei unterschiedliche Ansätze miteinander verglichen, die auf der Singulärwertzerlegung beziehungsweise der Anwendung der schnellen Fourier-Transformation auf interpolierten Beobachtungsdaten beruhen. Anhand von Tests mit simulierten Daten wird gezeigt, dass mit der Singulärwertzerlegung eine genauere Schätzung der Parameter möglich ist, während die Fourier-Transformation deutlich schneller ist. Für eine optimierte PSI-Auswertung wird deshalb eine Kombination beider Methoden in einem iterativen Ansatz realisiert.

Die Funktionalität der optimierten PSI-Auswertung wird anhand einer Anwendungsstudie getestet, bei der die Bodenbewegungen im Deformationsgebiet in Staufen (Breisgau) untersucht werden. Mit dem optimierten PSI-Ansatz können generell mehr PS-Punkte identifiziert werden, wobei in den Bereichen mit starken Bewegungsraten die Anzahl zuverlässiger PS-Punkte nahezu verdoppelt wird. Durch die robuste Parameterschätzung wer-

den insbesondere mehr Punkte an den Fassaden und auf den Dächern von Gebäuden identifiziert. Sie erlauben eine differenzierte Aussage über Gebäudeverkippungen. Zudem wird die systematische Unterschätzung der Bewegungsraten behoben, die bei dem Beispiel von Staufen mit der konventionellen PSI-Auswertung bisher aufgetreten ist.

Die Dissertation ist im Verzeichnis der Bibliothek des Karlsruher Institut für Technologie online verfügbar.

Mitteilung der DGPF

Ehrendoktorwürde für Prof. em. Dr. Armin Grün

Im Rahmen einer akademischen Feier wurde am 21. September 2015 Prof. em. Dr. Armin Grün, ETH Zürich, von der Aristotle University Thessaloniki die Würde eines Ehrendoktors (Dr. h.c.) überreicht. Damit wurden seine hervorragenden Leistungen in der Photogrammetry und Fernerkundung gewürdigt. Die Laudatio wurde gehalten von Prof. Petros Patias. Grün bedankte sich mit einem Vortrag zum Thema „Everything moves".

Im Rahmen dieser Veranstaltung wurde am nächsten Tag (22. September) ein Kolloquium zum Thema „Trends in Photogrammetry" durchgeführt, bei dem 14 Wissenschaftler ihre Forschungsarbeiten mit einem breiten Spektrum von Themen vorstellten.

Abb: Prof. Grün mit dem Rektor der Universität Prof. Periklis A. Mitkas.

Veranstaltungskalender

2016

10. – 12. Februar: **EuroCOW 2016** in **Lausanne**, Schweiz. eurocow2016.org

20. – 22. April: **Interexpo Geo-Siberia 2016** in **Novosibirsk**, Russland. http://expo-geo.ru/event/4-Interekspo_GEO-SIBIR

9. – 13. Mai: **Living Planet Symposium 2016** in **Prag**, Tschechien. http://lps16.esa.int

10. – 11. Mai: **Internationales 3D-Forum Lindau 2016** in **Lindau**. 3d-forum.li

6. – 9. Juni: **EUSAR 2016 – 11th European Conference on Synthetic Aperture Radar** in **Hamburg**. eusar.de

14. – 16. Juni: **geoinfo.potsdam.2016** in **Potsdam**. www.geoinfo.dgfk.net

26. Juni – 1. Juli: **CVPR 2016 – International Conference on Computer Vision and Pattern Recognition 2016** in **Las Vegas**, USA. pamitc.org/cvpr16

10. – 15. Juli: **IGARSS 2016 – International Geoscience and Remote Sensing Symposium 2015** in **Peking**, China. igarss2016.org

12. – 19. Juli: **ISPRS Congress 2016** in **Prag**, Tschechien. www.isprs2016-prague.com

14. – 16. September: **GEOBIA 2016** in **Enschede**, Niederlande. geobia2016.com

22. – 23. September: **2nd Virtual Geoscience Conference (VGC 2016)** in **Bergen**, Norwegen. virtualoutcrop.com/vgc2016

25. – 28. September: **ICIP 2016 – International Conference on Image Processing 2016** in **Phoenix**, USA. ieeeicip2016.org

10. – 16. Oktober: **ECCV 2016 – European Conference on Computer Vision 2016** in **Amsterdam**, Niederlande. eccv2016.org

11. – 13. Oktober: **Intergeo 2016** in **Hamburg**. intergeo.de

8. – 11. November: **ICPR 2016 – International Conference on Pattern Recognition 2016** in **Cancun**, Mexiko. icpr2016.org

Weitere Konferenzen und Workshops finden sich beispielsweise unter:
isprs.org/calendar/Default.aspx
conferences.visionbib.com

Korporative Mitglieder

Firmen

AEROWEST GmbH
AICON 3D Systems GmbH
Airbus DS Geo GmbH
aphos Leipzig AG
ASTEC GEODATA GmbH
Bernhard Harzer Verlag GmbH
Black Bridge AG
Blom Deutschland GmbH
Brockmann Consult GmbH
bsf swissphoto GmbH
Büro Immekus
DB Netz AG
DELPHI IMM GmbH
Deutsches Bergbau-Museum
EFTAS Fernerkundung Technologietransfer GmbH
ESG Elektroniksystem- und Logistik-GmbH
Esri Deutschland GmbH
EUROPEAN SPACE IMAGING
Eurosense GmbH
Exelis Visual Information Solutions GmbH
fokus GmbH
GAF GmbH
GeoCart Herten GmbH
Geoinform. & Photogr. Engin. Dr. Kruck & Co. GbR
geoplana Ingenieurgesellschaft mbH
GEOSYSTEMS GmbH
GGS - Büro für Geotechnik, Geoinformatik, Service
Hansa Luftbild AG
Herbert Wichmann, VDE Verlag GmbH
IAGB mbH
IGI – Ingenieur-Gesellschaft für Interfaces mbH
ILV-Fernerkundungs GmbH
INVERS – Industrievermessung & Systeme
Leica Geosystems GmbH
Linsinger ZT GmbH
Luftbilddatenbank Dr. Carls GmbH
map/x/tek
Messbildstelle GmbH
Microsoft Photogrammetry
MILAN Geoservice GmbH
M.O.S.S. Computer Grafik Systeme GmbH
PHOENICS GmbH
PMS – Photo Mess Systeme AG
RIEGL Laser Measurement Systems GmbH
RWE Power AG, Geobasisdaten/Markscheidewesen
technet GmbH
Terra-Messflug GmbH
TRIGIS GmbH
Trimble Germany GmbH
trimetric 3D Service GmbH
Z/I Imaging Ltd.

Behörden

Bayerische Landesanstalt für Wald und Forstwirtschaft
Bundesamt für Kartographie und Geodäsie
Bundesministerium für Ernährung, Landwirtschaft und Verbraucherschutz
Hessisches LA für Bodenmanagement und Geoinformation
Innenministerium NRW, Gruppe Vermessungswesen
Institut für Umwelt- und Zukunftsforschung
LA für Geoinformation und Landentwicklung, BW
LA für Digitalisierung, Breitband und Vermessung, Bayern
LA für Vermessung und Geoinformation, Schleswig-Holstein
LB Geoinformation und Vermessung, Hamburg
LB für Küstenschutz, Nationalpark und Meeresschutz, SH
Landeshauptstadt Düsseldorf, Vermessungs- und Liegenschaftsamt
Landesvermessung und Geobasisinformation Niedersachsen
Märkischer Kreis, Vermessungs- und Katasteramt
Regierungspräsident Tübingen, Abt. 8 Forstdirektion
Regionalverband Ruhr
Staatsbetrieb Sachsenforst
Stadt Köln, Amt für Liegenschaften, Vermessung und Kataster
Stadt Wuppertal, Vermessung, Katasteramt und Geodaten
Thüringer LA für Vermessung und Geoinformation
Zentrum für Geoinformationswesen der Bundeswehr

Hochschulen

BTU Cottbus, Lehrstuhl für Vermessungskunde
FH Frankfurt a.M., FB 1, Studiengang Geoinformation
FH Mainz, Institut für Raumbezogene Informations- und Messtechnik
HCU HafenCity Universität Hamburg, Geomatik
HfT Stuttgart, Vermessung und Geoinformatik
HS Bochum, FB Vermessung und Geoinformatik
HS Karlsruhe, Fakultät für Geomatik
HTW Dresden, FB Vermessungswesen/Kartographie
Jade Hochschule, Institut für Angewandte Photogrammetrie und Geoinformatik
LUH Hannover, Institut für Kartographie und Geoinformatik
LUH Hannover, Institut für Photogrammetrie und Geoinformation
MLU Halle, FG Geofernerkundung
Rhein Ahr Campus, Anwendungszentrum für multimodale und luftgestützte Sensorik
Ruhr-Uni Bochum, Geographisches Institut
RWTH Aachen, Geodätisches Institut
TU Bergakademie Freiberg, Institut für Markscheidewesen und Geodäsie
TU Berlin, Computer Vision & Remote Sensing
TU Berlin, Institut für Geodäsie und Geoinformationstechnik
TU Braunschweig, Institut für Geodäsie und Photogrammetrie
TU Clausthal, Institut für Geotechnik und Markscheidewesen
TU Darmstadt, Institut für Geodäsie, FG Fernerkundung und Bildanalyse
TU Dresden, Institut für Photogrammetrie und Fernerkundung
TU München, FG Photogrammetrie und Fernerkundung
TU München, Lehrstuhl für Geoinformatik
TU Wien, FG Photogrammetrie und Fernerkundung
Uni Bonn, Institut für Photogrammetrie
Uni Göttingen, Abt. Waldinventur und Fernerkundung
Uni Kassel, FG Grünlandwissenschaften und Rohstoffe
Uni Kiel, Geographisches Institut
Uni Stuttgart, Institut für Photogrammetrie
Uni Trier, Institut für Umweltfernerkundung und Geoinformatik
Uni Würzburg, Geographisches Institut
Uni zu Köln, Geographisches Institut